UiO : Department of Mathematics
University of Oslo

Long Wave Runup

A Numerical Investigation of Breaking and Non-breaking Waves on Composite Slopes

Christian Pedersen

Master's Thesis, Spring 2017

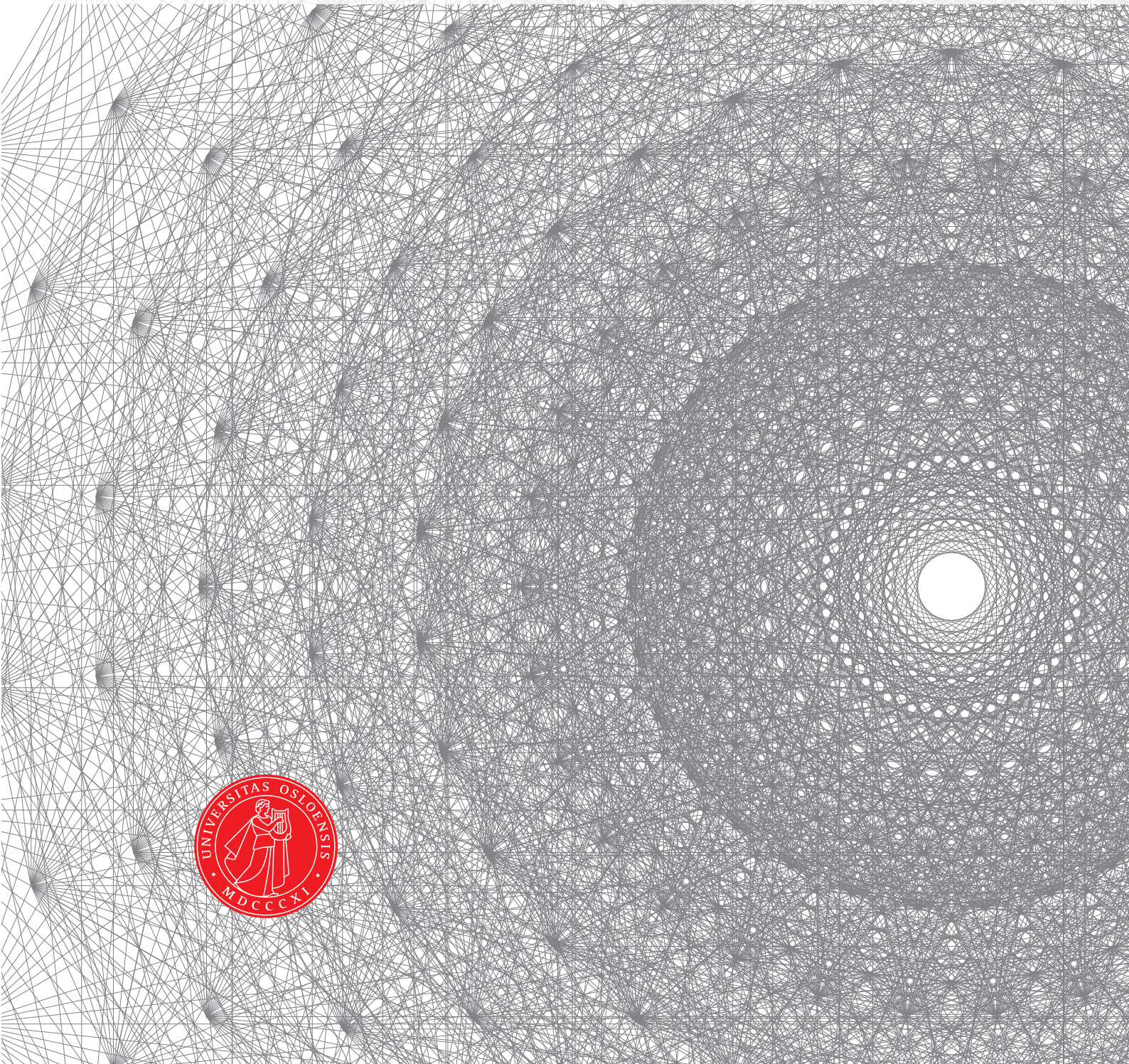

This master's thesis is submitted under the master's programme *Computational Science and Engineering*, with programme option *Computational Science*, at the Department of Mathematics, University of Oslo. The scope of the thesis is 60 credits.

The front page depicts a section of the root system of the exceptional Lie group E_8, projected into the plane. Lie groups were invented by the Norwegian mathematician Sophus Lie (1842–1899) to express symmetries in differential equations and today they play a central role in various parts of mathematics.

Abstract

In this thesis results from numerical simulations of long wave run-up on composite beaches are presented along with the analytical solution to the linear problem. The purpose of this study is to find out which parts of the slope are crucial with respect to the angles. The numerical models used are based on non-dispersive shallow water theory in which an essential assumption is that the wavelength is large compared to the depth. The results suggest that the linear run-up height on a composite slope can to a great extent be estimated analytically by the parameters describing the slope segment closest to the shoreline. For nonlinear waves the results are divided into categories. For strictly non-breaking waves the run-up height is found to be similar to the linear run-up height. It was found to be higher if the incident waves had a steep wavefront. For breaking waves the run-up height was found to be much lower. This is due to the dissipation of energy during the breaking process. However, the results suggests that even for breaking waves the run-up height is determined by the slope parameters in the region where the depth approaches zero.

Acknowledgements

First of all I would like to thank my supervisor professor Geir Pedersen. Without your support and guidance I would not have been able to write this thesis. I am very grateful for all you have taught me and for not ever letting me skip any steps in my reasoning. You were always available for questions and conversations about relevant (and very often not relevant) topics and your knowledge about Sumerian gods, flute in rock music and the meaning of Turkish family names is almost as impressive as your knowledge about fluid mechanics.

I also want to thank associate professor Marius Lysebo at HiOA, who inspired me to pursue this master degree. After all, you are the one who made me realize that life is much more enjoyable if you understand how things work. I also want to thank the great bunch of people in room 925 and especially Greger Svenn who joined me on this journey all the way from HiOA.

Finally I must thank the fabulous Kristine Aas for putting up with me being a student for as long as I have and for (most of the time) pretending to listen to me babbling about things you had no interest of hearing.

Christian Pedersen
Oslo, 29. May 2017

Contents

Chapter 1

Introduction

1.1 Why do we need run-up models?

Tsunamis are one of the most destructive and deadly natural disasters in the world. The wave run-up on beaches and structures is the final, and most important, issue from a hazard point of view. A tsunami is a sea wave created by a huge displacement of water, usually generated by earthquakes or landslides and they can travel large distances in open water with hardly any loss of energy (see figure 1.1 for illustration). A tsunami is considered to be a long wave, or a shallow water wave, meaning that its wavelength is large and its amplitude is small compared to the ocean depth. As a tsunami reaches the coastline it's amplitude increases and it can travel inland and cause major structural damage and loss of life.

Recent major tsunamis are the 2004 Indian Ocean tsunami that was created by an underwater earthquake, traveling thousands of kilometers and taking over 200.000 lives. Another example is the 2011 Tohoku earthquake causing a tsunami to hit the east coast of Japan with the highest recorded impact amplitude of 40.5 meters, causing over 18.000 deaths and major structural damage leading to the nuclear meltdown of the Fukushima Nuclear Power Plant. Incidents like these points out the importance of a better understanding of this final and crucial step that is the wave run-up to improve our ability to predict the coastal impact of tsunamis.

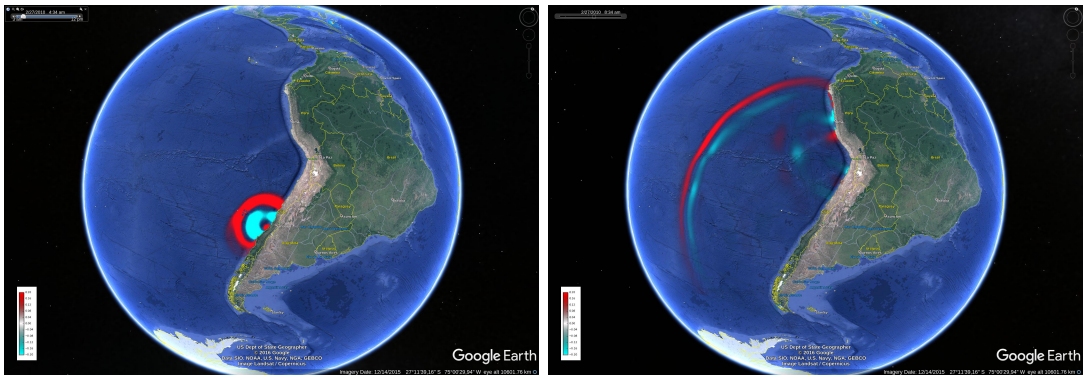

Figure 1.1: Images from a simulation of the 2010 Chile tsunami using the CLAW-Pack software [23] displayed in Google Earth [6]. The tsunami was created by an earthquake south west of Santiago at 3:34 am on the 27/2/2010. Left image depicts the wave 1 hour after the earthquake and the right image depicts the wave 4 hours later.

1.2 Previous work and motivation

Long wave run-up is well studied field yet it still have many unanswered questions. Pedersen and Gjevik [17] presented a numerical model developed to study run-up of long non-breaking waves described by the Boussinesq equations. For steep beaches the results showed good agreement with experiments but for beaches with a lower incline the numerical results overestimated the run-up height R. They suggested that this might be caused partly by neglecting bottom friction in the numerical solver. Pedersen [18] presented a numerical study of the linear run-up problem for periodic waves on a straight beach. He reported on the relative run-up amplitude R/a_0 where R is the run-up height and a_0 is the amplitude of the incident wave. He showed that R/a_0 could be expressed as a function only dependent on the wavelength, λ, of the incident wave. The run-up height function yielded stationary infliction point, i.e. the same run-up height was obtained for several values of λ. The results also showed that for waves with and oblique angle of incidence, these infliction points would turn into extrema. Synolakis [22] studied run-up of non-breaking and breaking waves. He derived asymptotic solutions to the run-up problem and found a breaking parameter a_0/h_0, where h_0 is the equilibrium water depth, which described the ratio for which a wave would break given a slope of a certain incline. His results matched the findings of Pedersen and Gjevik and he showed that some non-breaking waves could achieve a run-up height which exceeded the linear run-up height given a certain ratio a_0/h_0. An extension of this study was performed by Kânoğlu and Synolakis [7] for run-up of solitary waves

on a composite slope. The results showed that the run-up height for strictly non-breaking waves are not affected by the first slope segments until the ratio h_1/h_0, where h_1 is the height of the first slope segment, was relatively large. His study only included solitary waves of two different amplitudes which gave the ratios $h_1/h_0 = 0.5, 0.7$ for the shortest and longest wave respectively. in addition to the run-up height, a recent paper by Pedersen [13] contains a discussion about the reflection that occurs from the discontinuous vertex created when connecting the constant depth region to the slope when performing the numerical simulation. A linear relation between the reflected amplitude and the incident waves wavelength are reported. Numerous other articles have been published on the topic and many of them have been covered in review papers by Pelinovsky and Mazova [19], Pedersen [14] and Madsen, Fuhrman, and Schäffer [11].

The mentioned articles all report on the run-up height of long waves, but very often only for specific bathymetries or certain wave parameters. A thorough study where vast amounts of parameters are tested to obtain quantitative answers into which parts of a composite slope is crucial when it comes to the run-up height has not yet been performed to the authors knowledge.

This thesis will investigate the run-up of linear periodic waves, linear single waves and non-linear single waves. In the non-linear case both breaking and non-breaking waves will be investigated. An open source NLSW solver, GeoClaw [23], will be used in the non-linear case which makes it possible to include bottom friction to the equations.

We seek out to obtain a deeper insight into the world of long wave run-up.

1.3 Contents of this thesis

This thesis is divided into four main parts

In chapter 2 a formulation of the shallow water equations are presented. A general scaling of parameters are introduced and the equations are simplified by linearizing and a phase plane formulation is developed. Optics are presented briefly as the validity of an optic approximation are discussed in the coming chapter.

In chapter 3 the analytical solutions of the run-up height for the linearized shallow water equations (LSW) for periodic waves are presented in great detail. Asymptotic run-up height are found and they match the optic approximation which is shown to be valid closer to the shoreline than expected. A suitable wave shape for this thesis is presented along with a breaking criterion. Finally we introduce the

composite slope of interest in this thesis.

Chapter 4 and 5 covers a description of the numerical models together with verification and validation. Refinement studies are performed for all solvers.

Chapter 6 and 7 are the result chapters of this thesis. In chapter 6 we present the results connected to reflection caused by changes in the bathymetry. A linear relation between the reflected waves amplitude and the incident wavelength as presented by Pedersen [13] is found to be valid for waves with short wavelengths relative to the slope. It is also found that employing a smooth transition between the offshore region and the slope has no noticeable effect on the run-up height for linear waves.

In chapter 7 the results of the run-up height simulations are presented. The run-up height for linear periodic waves are found to be unaffected by the first slope segment for a large ratio h_1/h_0. However the occurrence of extrema make it hard to draw exact conclusions in the general case. For linear single waves the results are more conclusive. The h_1/h_0 ratio found by Kânoğlu and Synolakis are confirmed even though the waves used in their study was much longer than the ones used in this thesis For nonlinear waves the run-up height is dependent on many parameters. However, in the case of a strictly non-breaking wave, the run-up height is similar to the linear one. It is shown that the steepness of the wave when it enters the slope is important for the run-up height. A steep non-breaking wave will result in increased run-up height. If the wave breaks the run-up height will decrease. However, inclusion of the friction term always results in lower run-up height than the linear for waves of equal ratio a_0/h_0.

In chapter 8 the conclusion of this thesis is presented along with suggestions for future work.

Chapter 2

Mathematical Formulation

2.1 The shallow water equations

The nonlinear shallow water equations is a set of partial differential equations

$$\frac{\partial \mathbf{u}^*}{\partial t^*} + \mathbf{u}^* \frac{\partial \mathbf{u}^*}{\partial \mathbf{x}^*} = -g^* \frac{\partial \eta^*}{\partial \mathbf{x}^*} \tag{2.1}$$

$$\frac{\partial \eta^*}{\partial t^*} = -\frac{\partial}{\partial \mathbf{x}^*} \left(\mathbf{u}^* \left(h^* + \eta^* \right) \right) \tag{2.2}$$

where $\mathbf{u}^*$ is the horizontal velocity, η^* is the surface elevation, $h^*(\mathbf{x}^*)$ is the unperturbed water depth and g^* is the gravitational acceleration. The asterisk indicates dimensional quantities. (2.1) is the equation of motion and (2.2) is the continuity equation. The equations are obtained by canceling the dispersive terms in the Boussinesq equations which is a commonly used description for propagating long waves. In shallow water theory, the horizontal velocity is vertically uniform and the pressure is hydrostatic [14]. Inherent in the name, a requirement for the theory is that the waves must be long relative to the water depth. This is expressed as

$$k^* h^* \ll 1 \tag{2.3}$$

where k^* is the wavenumber.

By introducing a characteristic water depth h_0 and a problem dependent characteristic horizontal length x_c, a set of non-dimensional variables are defined as

$$\begin{aligned} \eta &= \frac{\eta^*}{h_0}\,, \qquad u = \frac{u^*}{\sqrt{g^* h_0}}\,, \qquad h = \frac{h^*}{h_0} \\ x &= \frac{x^*}{x_c}\,, \qquad t = \frac{t^*}{x_c}\sqrt{g^* h_0} \end{aligned} \tag{2.4}$$

The time scale is thus given as $t_c = x_c/\sqrt{g^* h_0}$. When inserting these variables into (2.1) and (2.2) we obtain the scaled nonlinear shallow water equations (NLSW)

$$\frac{\partial \mathbf{u}}{\partial t} + \mathbf{u}\frac{\partial \mathbf{u}}{\partial \mathbf{x}} = -\frac{\partial \eta}{\partial \mathbf{x}} \tag{2.5}$$

$$\frac{\partial \eta}{\partial t} = -\frac{\partial}{\partial \mathbf{x}}\left(\mathbf{u}\left(h+\eta\right)\right) \tag{2.6}$$

For a constant depth bathymetry, the non-dimensional phase velocity is for the NLSW defined as

$$c = \sqrt{1+\eta} \tag{2.7}$$

2.2 The linearized shallow water equations

To determine which parameters are crucial when it comes to wave run-up, it is important to be able to make calculations for sufficient parameter combinations. The best way to achieve this is to simplify the equations at hand. Pedersen & Gjevik [5] showed that for non breaking waves, the ratio between the run-up height R and the initial amplitude a_0 of the incoming waves is not affected by nonlinearity. A trait of these waves is that their amplitude is small compared to the depth which is expressed as

$$\frac{\eta^*}{h^*} \ll 1 \tag{2.8}$$

For such waves the NLSW can be linearized and we obtain the scaled linear shallow water equations (LSW)

$$\frac{\partial u}{\partial t} = -\frac{\partial \eta}{\partial x} \tag{2.9}$$

$$\frac{\partial \eta}{\partial t} = -\frac{\partial uh}{\partial x} \tag{2.10}$$

By taking the spatial derivative of (2.9) and substituting with (2.10) we can eliminate the velocity and the LSW can be rewritten as

$$\frac{\partial^2 \eta}{\partial t^2} - \frac{\partial}{\partial x}\left(h(x)\frac{\partial \eta}{\partial x}\right) = 0 \tag{2.11}$$

which is the standard wave equation for non-dispersive plane waves with a variable depth coefficient. For a constant depth h_0, LSW have sinusoidal solutions

$$\eta(x,t) = f\left(x - c_0 t\right) + g\left(x + c_0 t\right) \tag{2.12}$$

$$u(x,t) = \frac{1}{c_0}\left(f\left(x - c_0 t\right) - g\left(x + c_0 t\right)\right) \tag{2.13}$$

where $c_0 = 1$ is the phase velocity. When compared to the non-linear phase velocity, we see that linearizing the equations is a reasonable approximation when $\eta \to 0$.

2.3 Phase plane formulation

To display certain characteristics of the LSW we can utilize the phase plane where only the spatial variables constitutes the coordinate system. We introduce a wave solution which is periodic in time

$$\eta(x,t) = \hat{\eta}(x)e^{-i\omega t} \tag{2.14}$$

where ω is the dimensionless angular frequency defined as

$$\omega = \omega^* t_c = \frac{2\pi}{\lambda}\sqrt{h(x)} \tag{2.15}$$

and $\lambda = \lambda^*/x_c$ is the offshore wave length. By inserting (2.14) into the standard wave equation (2.11) the time dependence can be separated out from the equation and we obtain

$$\frac{d}{dx}\left(h(x)\frac{d\hat{\eta}}{dx}\right) + \omega^2\hat{\eta} = 0 \tag{2.16}$$

2.4 Optics

Optics is the description of light as electromagnetic waves. For linear periodic waves the comparison with optics is often used even though important water wave behavior, such as reflection along the rays, is not a property of electromagnetic waves. The optic description of a shoaling water wave is clearly not valid beyond the shoreline but at what point during the run-up process the comparison fails is to the authors knowledge not well defined in literature. A minimalistic introduction to the optic properties needed in this thesis is presented below.

Assume that the surface elevation in an inhomogeneous medium can be expressed as

$$\eta(x,t) = A(x,t)e^{i\chi(x,t)} \tag{2.17}$$

where χ is the phase function and A is the amplitude. From the phase function we can define the wavenumber k and ω as

$$k = \nabla\chi\,, \qquad \omega = \pm\frac{d\chi}{dt} \tag{2.18}$$

For optics to be valid, the coefficients A, k and ω must be slowly varying functions of time and space, i.e. that they change little over a defined distance or time such as the wavelength or wave period. Both k and ω must fulfill the dispersion relation which for shallow water waves reads

$$\omega = k\sqrt{h(x)} \tag{2.19}$$

If ω is constant in time the phase function is then defined as

$$\chi = \int k dx = \int \frac{\omega}{\sqrt{h(x)}} dx \tag{2.20}$$

If there is no external energy input, such as wind or currents, the sum of energy fluxes into a domain must equal the change in energy density inside the domain which is expressed as

$$\frac{\partial E}{\partial t} + \nabla \cdot (c_g E) = 0 \tag{2.21}$$

with $c_g = \sqrt{h(x)}$ being the group velocity. From [4] we have that the energy density is proportional to the wave amplitude squared. For a periodic wave train we can thus find the amplitude through the now simplified (2.21)

$$\nabla \cdot (c_g A^2) = 0 \tag{2.22}$$

For simple geometries this integral equation can easily be solved, but for more complex geometries the constants can be determined through numerical solutions of (2.16).

Chapter 3

Analytical Solutions and Useful Parameters

A comprehensive amount of research has been done to find analytical solutions for the wave run-up phenomena over the years. Madsen et al. [11] and Pelonovsky et al.[19] reviews the most applicable solutions in an easy manner. In this chapter the run-up height solution obtained by the linear phase plane formulation will be covered in great detail since the solution and reasoning are important for this thesis. In the nonlinear case only certain characteristics and parameters for a traveling wave will be discussed. Finally we introduce the composite slope used in this thesis together with all its the relevant parameters.

3.1 Runup height on a single inclined plane

Introducing a simple geometry as shown in figure 3.1. We define the offshore area where $x^* < x_k^*$ and the near-shore area where $x_k^* \leq x^* \leq x_S^*$. The length of the near-shore area is defined as L^*. Now we define the characteristic horizontal length by introducing a scaling criterion

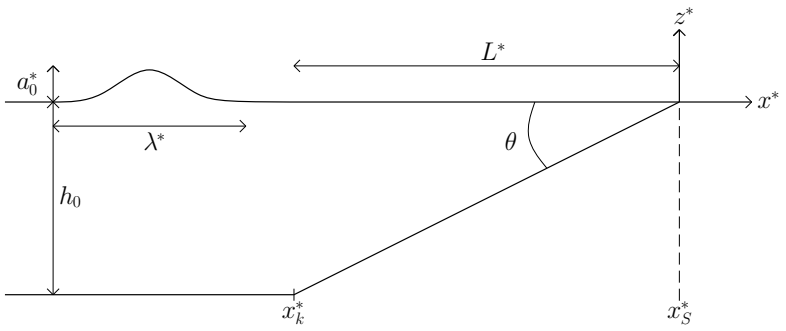

Figure 3.1: Bathymetry with a single inclined plane. All variables have dimension except θ.

$$\frac{dh}{dx} = 1 \,, \qquad x_k \leq x \leq x_S \tag{3.1}$$

which yields $x_c = h_0 \cot(\theta) = 1$. By scaling all vertical parameters by h_0 and all horizontal parameters by x_c the unperturbed dimensionless water depth in the near-shore area is defined as

$$h(x) = |x - x_S| \tag{3.2}$$

For this bathymetry the equation (2.16) reads

$$\frac{d}{dx}\left(|x - x_S|\frac{d\hat{\eta}}{dx}\right) + \omega^2\hat{\eta} = 0 \tag{3.3}$$

This is known as the Sturm-Liouville equation and it has two solutions besides the trivial one [22]. However, one of these solution is infinite at the shoreline and must be excluded. The solution then reads

$$\hat{\eta}(x) = RJ_0(\sigma) \tag{3.4}$$

where R is the run-up height and J_0 is the zeroth order Bessel function of the first kind with argument

$$\sigma = 2\omega\sqrt{|x - x_S|} \tag{3.5}$$

In the offshore region, the incoming wave is defined as

$$\hat{\eta}_i(x) = a_0 e^{ik(x - x_k)} \tag{3.6}$$

and the reflected wave due to the sloping hill is defined as

$$\hat{\eta}_r(x) = a_r e^{-ik(x-x_k)} \tag{3.7}$$

where the wavenumber k is given by the dispersion relation $\omega = k$. a_0 and a_r are the incoming waves amplitude and the reflected amplitude respectively. In order to determine the run-up height and the reflected amplitude coefficients, the near-shore solution and the offshore solutions is matched where the two regions meet. Hence, the conditions of continuity of momentum and mass flux

$$\frac{d\left(\hat{\eta}_i + \hat{\eta}_r\right)}{dx} = \frac{d\hat{\eta}}{dx}\,, \qquad \hat{\eta}_i + \hat{\eta}_r = \hat{\eta} \tag{3.8}$$

is applied at $x = x_k$. This yields the coefficients

$$a_r = a_0 \left(\frac{J_0(\sigma_k) + iJ_1(\sigma_k)}{J_0(\sigma_k) - iJ_1(\sigma_k)} \right) \tag{3.9}$$

$$R = \frac{2a_0}{J_0(\sigma_k) - iJ_1(\sigma_k)} \tag{3.10}$$

where σ_k is σ evaluated at $x = x_k$

$$\sigma_k = \frac{4\pi}{\lambda} \tag{3.11}$$

With the scaling implemented for this bathymetry, consisting of a single inclined plane, the run-up height is only dependent on the initial wavelength λ. With R being a complex number the maximum run-up amplitude can be found in the magnitude of R

$$|R| = \frac{2a_0}{\sqrt{J_0^2(\sigma_k) + J_1^2(\sigma_k)}} \tag{3.12}$$

When $\lambda \to \infty$, $\sigma \to 0$ and the maximum run-up amplitude $|R| \to 2a_0$ which is coherent with a wave hitting a vertical wall.

Far away from the shoreline, i.e. when $\sigma \gg 1$, a leading order asymptotic approximation for the Bessel function [20] is expressed as

$$
\begin{aligned}
J_0(\sigma) &\sim \sqrt{\frac{2}{\sigma\pi}}\cos\left(\sigma - \frac{\pi}{4}\right) \\
J_1(\sigma) &\sim \sqrt{\frac{2}{\sigma\pi}}\sin\left(\sigma - \frac{\pi}{4}\right)
\end{aligned}
\tag{3.13}
$$

We observe that with these approximations the amplitude will be a function of $h(x)^{-1/4}$ which is in accordance with Green's law for non-breaking surface waves in shallow water [21]. This also means that the approximation is not valid at the shoreline since the solution becomes singular when $h(x) = 0$. By utilizing these approximations in (3.10) a simplified relation between the run-up height and the amplitude of the incoming wave can be expressed as

$$
\frac{R}{a_0} = \sqrt{2\pi\sigma_k} \tag{3.14}
$$

In figure 3.2 we can see that the approximation is in compliance with (3.12) for wave lengths shorter than the near-shore region. This is consistent with the findings of Didenkulova [3].

The rescaled solution to the problem is included to ease the comparison with published literature

$$
\eta^*(x^*) = R^* J_0\left(2\omega^*\sqrt{\frac{|x^* - x_S^*|}{g^*\tan(\theta)}}\right) \tag{3.15}
$$

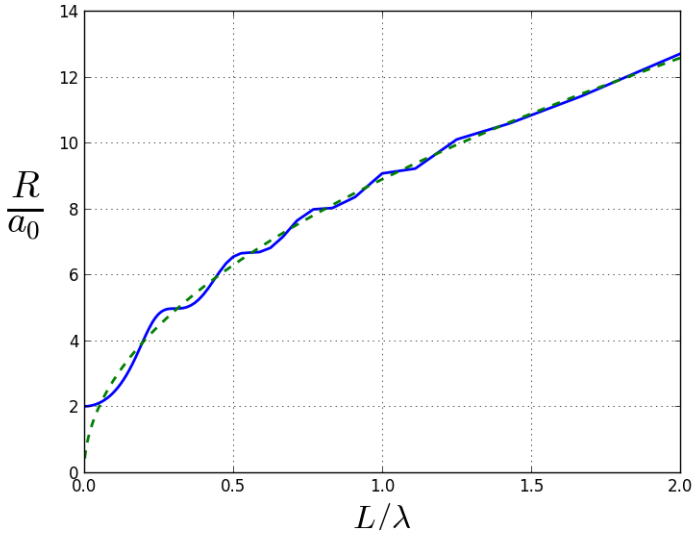

Figure 3.2: Relative run-up amplitude. The solid line represents the exact solution (3.12) and the dashed line the approximation (3.14).

3.2 Optic approximation

We employ a near-shore solution on the form

$$\eta_{optic}(x) = A(x)e^{i\chi(x)} \tag{3.16}$$

For the bathymetry in figure 3.1 we find the phase function according to (2.20) as

$$\chi = 2\omega\sqrt{|x - x_S|} + \chi_0 \tag{3.17}$$

and the amplitude is determined by (2.22)

$$A = Ch(x)^{-1/4} \tag{3.18}$$

where χ_0 and C are constants that needs to be found. Notice that the solution is singular at the shoreline and thus not valid when $h(x) = 0$. For this geometry the constant are already found in the previous section and the solution reads

$$\eta_{optic}(x) = \frac{a_0}{\pi}\left(\frac{\lambda^2|x - x_S|}{4}\right)^{-1/4} e^{i\left(2\omega\sqrt{|x-x_S|}-\frac{\pi}{4}\right)} \tag{3.19}$$

The solution was easily derived for a simple geometry such as a single inclined plane. However for a more complex geometry the derivation would become cumbersome and tedious and sometimes even impossible for many bottom profiles. For such bathymetries the constants χ_0 and C would most easily be derived by matching with the numerical solution of (2.16)

In figure 3.3 the optic approximation (3.19) is compared to the exact solution (3.12) and is shown as a relative difference defined as

$$RD_{optic} = 1 - \frac{\eta_{optic}}{\eta_{exact}} \tag{3.20}$$

We observe minor discrepancies between the approximation and the exact solution when the depth is large. This is likely due the lack of reflection in the approximate solution and thus the phase is slightly off. The comparison shows that the optic approximation (3.16) for the single inclined plane bathymetry is very accurate remarkably close to the shoreline. The depth where the relative difference first exceeds 5% is less than 1% of the waves offshore wave length.

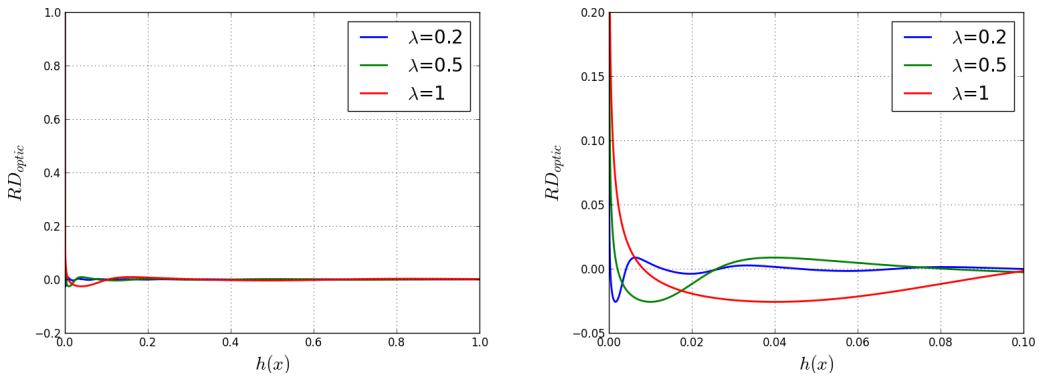

Figure 3.3: The relative difference (3.20) between optic approximation (3.16) and exact solution (3.12). Right image is a cropped version of the left image.

3.3 Nonlinear effects on traveling waves

Before introducing our traveling wave, we first present an updated sketch of our single inclined plane bathymetry in figure 3.4. The scaling are left unchanged.

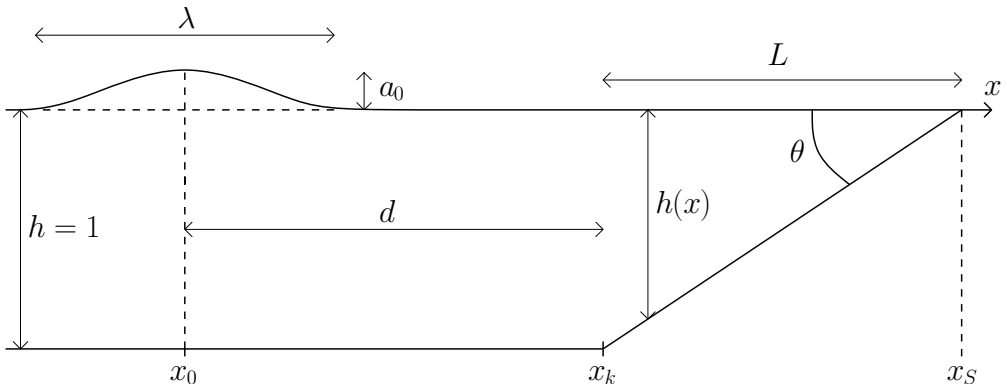

Figure 3.4: Incident wave propagating towards the shoreline over a plane inclined slope. All variables are dimensionless.

Depicted in the figure are a single traveling wave with initial wavelength λ and amplitude a_0. In this thesis an initial wave shape centered around $x_0 = 0$ at time $t = 0$ is chosen to be on the form

$$\eta = a_0 \operatorname{sech}^2(kx) \tag{3.21}$$

This wave shape is smooth [10], i.e it is infinitely differentiable, and it is a solitary wave if

$$k = k_{sol} = \sqrt{\frac{3a_0}{4}} \tag{3.22}$$

which is the solitary wave number described in [14]. However, in order to choose the amplitude and wavelength independently from one another, (3.22) will not be used and we need to define a suitable wavenumber. Since the wavelength of a long wave can be somewhat abstract, we define a wavelength as the distance between the two points on the surface elevation that corresponds to 10% of the waves maximum height. Hence, the wavenumber for the propagating wave is defined as

$$k = \frac{2\operatorname{sech}^{-1}(\sqrt{0.1})}{\lambda} \approx \frac{3.64}{\lambda} \tag{3.23}$$

In figure 3.5 the wave shape for a few selected wavelengths are compared to the solitary wave with a fixed $a_0 = 0.1$.

For the LSW, most parameters introduced in figure 3.4 are arbitrary as the equations are not dispersive nor nonlinear. Thus the distance d which the wave must

propagate before it reaches the inclined plane at x_k is of no importance. For the NLSW, the phase speed (2.7) is a function of the wave height and consequently the steepness of the wavefront might be heavily influenced by the length of d which in turn might affect the run-up height. To determine when the wavefront becomes so steep that the wave breaks, we introduce a breaking criteria for solitary waves derived by Synolakis in [22] on dimensional form

$$\frac{a_0^*}{h_0} < 0.479 \left(\tan(\theta)\right)^{\frac{10}{9}} \tag{3.24}$$

Inspired by Pedersen [14] we divide the criteria by $k^* h_0$ and utilize (3.22) to obtain a scaled criterion for the single inclined plane

$$a_0 < 1.332 k^{-\frac{5}{2}} \tag{3.25}$$

This breaking criteria can however only be treated as an approximate result and pointing out it's limitations is essential. The parameter is derived for a single inclined plane and it does not consider wave reflection from the connecting points in a composite slope. The steepening process whilst propagating the distance d is not considered, and of course, the chosen wave shape is not a solitary wave. Still, this has shown to provide the author with a fair estimate of which parameters to investigate. Two figures, B.2 and B.3, are included in the appendix depicting the breaking criteria (3.25) as a function of the wavelength for two different incline angles.

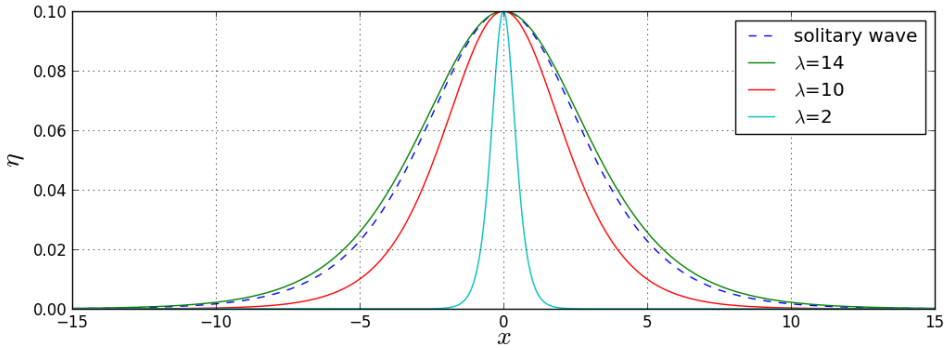

Figure 3.5: Shape of a single traveling wave with $a_0 = 0.1$. The dashed line represents the solitary wave shape (3.21) with $k = k_{sol}$. The solid lines represents (3.21) with wave number (3.23) for $\lambda = 2, 10, 14$.

3.4 Scaling for composite slopes

For a composite slopes bathymetry the scaling criteria (3.1) is per definition not applicable. So we introduce a new bathymetry consisting of two piecewise linear planes, depicted in figure 3.6.

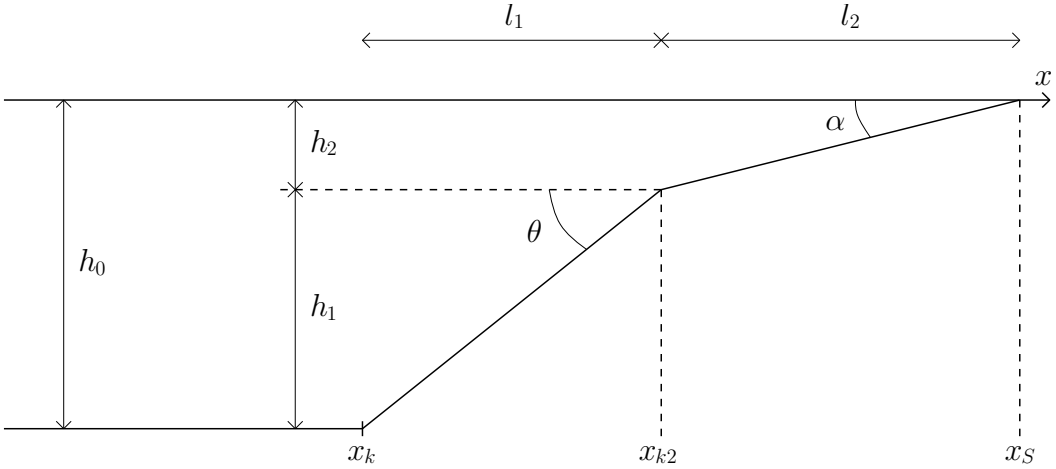

Figure 3.6: A bottom profile with two piecewise linear inclined planes.

The depth of this bottom profile is

$$h(x) = \begin{cases} 1, & \text{if } x < x_k \\ |x - x_{k2}| \tan(\theta) + h_2, & \text{if } x_k \leq x < x_{k2} \\ |x - x_S|\alpha, & \text{if } x_{k2} \leq x \leq x_S \end{cases} \tag{3.26}$$

where α is the incline of the second slope segment. A new scaling criteria is imposed on the first slope segment

$$\frac{dh}{dx} = 1 \,, \quad x_k \leq x \leq x_{k2} \tag{3.27}$$

yielding $x_c = h_0 \cot\theta = 1$ and $h_1 = l_1$. The location of x_{k2} is dependent on h_1 and thus the parameters that might influence the run-up height now include h_1 and α. We note that when $h_1 = 1$ we obtain the single inclined plane bathymetry depicted in figure 3.4.

An illustration of the geometry with all the parameters used in this thesis are included in appendix B (figure B.1) for easy access.

Chapter 4

Numerical Methods

4.1 Boundary conditions

In numerics, the spatial domain in which the wave is simulated is finite. For a linear problem with one horizontal coordinate the domain is bounded by the start of the offshore region and the shoreline. The main problem is the boundary at the shoreline. This boundary is dealt with by ensuring that the horizontal volume flux at this point is zero

$$uh\Big|_{x=x_S} = 0 \tag{4.1}$$

This is implemented by adjusting the discretization in such a way that the boundary mesh point of u is placed on the same mesh point where $h = 0$. The surface elevation at the shoreline can then be extrapolated by means of the nearby mesh point values.

The offshore/inlet boundary condition is dealt with differently for each solver and they consist of a reflective boundary condition

$$\frac{\partial \eta}{\partial x} = 0 \tag{4.2}$$

and a radiation or combined radiation/input condition

$$\frac{\partial \eta}{\partial t} \pm c\frac{\partial \eta}{\partial x} = B_0 \tag{4.3}$$

where B_0 is dependent on the initial condition. The discretization of the boundary conditions will be explained in the following sections.

4.2 LSW - time plane solver

The set of equations (2.10) and (2.9) is solved numerically by implementing a staggered grid [15] as can be seen in figure 4.1.

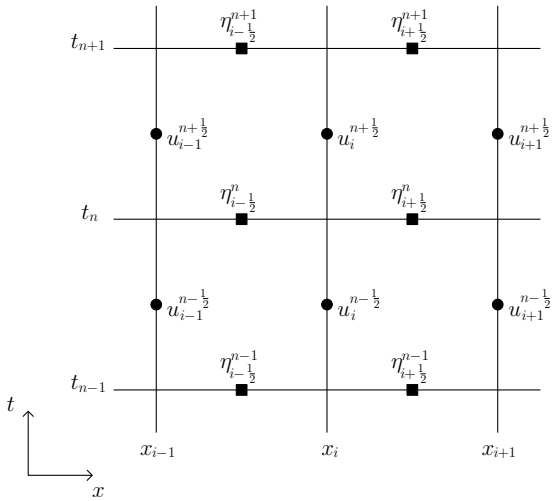

Figure 4.1: A random set of staggered grid molecules.

The grid is constructed of one time array and two spatial arrays, one for u and one for η. The spatial array for u consists of $N_x + 1$ uniformly spaced mesh points over the interval $x_L \leq x \leq x_R$ where x_L indicate the leftmost boundary which is by default set to $x_0 = 0$ and x_R is the rightmost boundary which is for run-up calculations $x_R = x_S$. The distance between each mesh point is separated by a length $\Delta x = \frac{x_R - x_L}{N_x}$ and a mesh point is then defined as $x_i = i\Delta x$ where $i = 0, ..., N_x + 1$.
The second spatial array consists of $N_x + 2$ mesh points. The first $N_x + 1$ points are uniformly spaced over the interval $x_L - \Delta x/2 \leq x \leq x_R - \Delta x/2$. The mesh points are here defined as $x_{i-\frac{1}{2}} = (i - \frac{1}{2})\Delta x$ where $i = 0, ..., N_x + 1$. The last mesh point is added at $x = x_R$ with a distance $\Delta x/2$ to the preceding mesh point.

The time array consists of N_t uniformly spaced mesh points over the interval $0 \leq t \leq T$. Each mesh point is separated by a distance $\Delta t = \frac{T}{N_t}$ which defines a temporal mesh point as $t_n = n\Delta t$ with $n = 0, ..., N_t$.

The two unknown variables are then defined as $\eta^n_{i-\frac{1}{2}} = \eta((i - \frac{1}{2})\Delta x,\ n\Delta t)$ and $u_i^{n+\frac{1}{2}} = u(i,\ (n + \frac{1}{2})\Delta t)$ and the discrete equations becomes

$$\frac{\eta^n_{i-\frac{1}{2}} - \eta^{n-1}_{i-\frac{1}{2}}}{\Delta t} = -\frac{h_i u_i^{n-\frac{1}{2}} - h_i u_{i-1}^{n-\frac{1}{2}}}{\Delta x} \tag{4.4}$$

$$\frac{u_i^{n+\frac{1}{2}} - u_i^{n-\frac{1}{2}}}{\Delta t} = -\frac{\eta^n_{i+\frac{1}{2}} - \eta^n_{i-\frac{1}{2}}}{\Delta x} \tag{4.5}$$

The calculation is initiated with an initial condition for η at $t = 0$ and a initial condition for u at $t = 0$ which is advanced half a time step. The time loop is then started by solving Eq.(4.4) for $\eta^n_{i-\frac{1}{2}}$ where $i = 1, ..., N_x + 1$. By ensuring that $h_{N_x+1} = 0$ the mesh point value for u_{N_x+1} is made redundant as the term vanishes from the equation. The value for η_{N_x+2} is then extrapolated using a second order Lagrange polynomial. The leftmost boundary value is calculated with a reflective boundary condition $\eta_{-\frac{1}{2}} = \eta_{\frac{1}{2}}$. Then the velocity equation (4.5) is solved for $u_i^{n+\frac{1}{2}}$ for $i = 0, ..., N_x + 1$ before the time step is advanced by Δt.

In the special case of a constant depth bathymetry, needed for testing the solver against an exact solution, the rightmost boundary is treated with a reflective boundary condition $\eta_{N_x+1} = \eta_{N_x+2}$. The same applies when testing against BMEP (see chapter 5) as this is the implemented boundary condition in that solver.

4.3 LSW - phase plane solver

For equation (2.16) the spatial domain is represented by one array for η values. The array consists of $N_x + 1$ uniformly spaced mesh points over the interval $x_L \leq x \leq x_R$. They are separated by a distance $\Delta x = \frac{x_R - x_L}{N_x}$ and a mesh point is then defined as $x_i = i\Delta x$ with $i = 0, ..., N_x + 1$.

The discrete form of equation (2.16) then becomes

$$\frac{h_{i+\frac{1}{2}}\left(\hat{\eta}_{i+1} - \hat{\eta}_i\right) - h_{i-\frac{1}{2}}\left(\hat{\eta}_i - \hat{\eta}_{i-1}\right)}{\Delta x^2} + \omega^2 \hat{\eta}_i = 0 \tag{4.6}$$

This can be solved as a set of linear equations $A\hat{\eta} = B$ where A is a tridiagonal matrix of size $N_x + 1 \times N_x + 1$ and η and B are vectors of length $N_x + 1$. The first and last row of A depends on the boundary conditions as does the first element of B.
The leftmost boundary is treated with a combined input/radiation condition which for a periodic wave solution is defined as

$$\frac{\hat{\eta}_1 - \hat{\eta}_0}{\Delta x} + \frac{ik_L}{2}(\hat{\eta}_1 + \hat{\eta}_0) = B_0 \tag{4.7}$$

where B_0 is derived in Eq.(4.3). By ensuring that $h_{N_x+1+\frac{1}{2}} = 0$ the need for the implementation of a numerical boundary condition at the shoreline is made redundant as the term for η_{N_x+1} vanishes from the equation. With this information the values of the matrix elements can be defined as

$$A = \frac{1}{\Delta x^2}\begin{bmatrix} b_0 & c_0 & 0 & \cdots & \cdots & \cdots & 0 \\ a_1 & b_1 & c_1 & \ddots & \ddots & \ddots & \vdots \\ 0 & \ddots & \ddots & \ddots & \ddots & \ddots & \vdots \\ \vdots & \ddots & a_i & b_i & c_i & \ddots & \vdots \\ \vdots & \ddots & \ddots & \ddots & \ddots & \ddots & 0 \\ \vdots & \ddots & \ddots & \ddots & a_{N_x} & b_{N_x} & c_{N_x} \\ 0 & \cdots & \cdots & \cdots & 0 & a_{N_x+1} & b_{N_x+1} \end{bmatrix} \tag{4.8}$$

where

$$\begin{aligned} a_0 &= 0\ , & b_0 &= \frac{ik_0\Delta x^2}{2} - \Delta x\ , & c_0 &= \frac{ik_1\Delta x^2}{2} + \Delta x \\ a_i &= h_{i-\frac{1}{2}}\ , & b_i &= \omega^2\Delta x^2 - h_{i+\frac{1}{2}} - h_{i-\frac{1}{2}}\ , & c_i &= h_{i+\frac{1}{2}} \\ a_{N_x+1} &= h_{i-\frac{1}{2}}\ , & b_{N_x+1} &= \omega^2\Delta x^2 - h_{i+\frac{1}{2}} - h_{i-\frac{1}{2}}\ , & c_{N_x+1} &= 0 \end{aligned} \tag{4.9}$$

and B is a zero vector except for the first element B_0.

In the special case of a constant depth bathymetry, needed to test the solver, the rightmost boundary is treated with a radiation boundary condition

$$\frac{\hat{\eta}_{N_x+1} - \hat{\eta}_{N_x}}{\Delta x} - \frac{ik}{2}(\hat{\eta}_{N_x+1} + \hat{\eta}_{N_x}) = 0 \tag{4.10}$$

yielding

$$\begin{aligned} a_{N_x+1} &= -\frac{ik_R\Delta x^2}{2} - \Delta x \\ b_{N_x+1} &= \Delta x - \frac{ik_R\Delta x^2}{2} \\ c_{N_x+1} &= 0 \end{aligned} \tag{4.11}$$

4.4 CLAWPack

CLAWPack stands for Conservation LAWs Package and it is a collection of finite volume methods for hyperbolic systems of conservation laws [23]. CLAWPack is an open source software with many contributors and a wide range of papers documenting and validating the solvers are published. The most relevant literature about CLAWPack for this thesis are published in [1], [9] and [8].

4.4.1 GeoClaw

CLAWPack as a collection has many different solvers, but for this thesis the GeoClaw solver is used. The GeoClaw solver is specially designed to handle geophysical problems such as the shallow water equations. Additional terms are added to the equations to include Coriolis forces and bottom friction. However, for problems in this thesis the Coriolis force is not included. When modeling inundation, including an appropriate bottom friction term is important. GeoClaw uses the Manning formulation in which the friction coefficient γ is by default set to $\gamma = 0.025$. For run-up calculations we will use this constant and compare it to a no-friction solution where $\gamma = 0$. For further details about the software, the reader is referred to the website *www.clawpack.org* [23] or the cited articles.

Chapter 5

Testing of Numerical Models

In this chapter the numerical schemes, i.e. the finite difference solvers, are tested against an exact solution or against another program solving the equations with the same discretization. We will perform two test cases which, for easy reference, is labeled

1. Case B1
   - Constant depth bathymetry with $h(x) = 1$
2. Case B2
   - Single inclined plane, presented in chapter 3 (Fig. 3.4)

Two error estimates are considered, the total error and the maximum error using the L^2 norm [24] and the L^∞ norm [25] respectively with the numerical error at each mesh point i defined as $e_i = |f_{exact}(x_i) - f_{numerical}(x_i)|$. In addition, refinement studies will be performed for all solvers, including the GeoClaw solver, to obtain a mesh resolution which yields a converged run-up height. The studies will be performed for the bathymetries constituting the "extremes" in this thesis, i.e. a composite slope with $h_1 = 0,1$ and $\alpha \approx 0.017$ which is the equivalent to an incline angle of 1°. For the LSW time plane solver a program (BMEP[1]) developed by Pedersen [15] for the standard Boussinesq equation is used for verification in the

[1]Boussinesq Model for Educational Purposes

inclined plane case.

5.1 LSW - Time plane solver

The numerical scheme for equations (4.4) and (4.5) has a second order error and it is stable for $\Delta t \leq \Delta x$. For $\Delta t = \Delta x$ the solver is exact. Verification can be seen in appendix A.1. As an exact solution of the surface elevation η for LSW, a Gaussian wave solution was chosen

$$G(x,t) = a_0 e^{-\left(\frac{x-x_0-t}{\lambda}\right)^2} \tag{5.1}$$

5.1.1 Test results

For case B1 two tests was performed with ratios $\frac{\Delta t}{\Delta x} = 0.8, 0.5$. Wave parameters for both simulations are $\lambda = 1.1$ and $a_0 = 0.5$ and the results are shown in table 5.1 and 5.2 respectively. The convergence rate depicted are for the last refinement step. Both tests shows a quadratic convergence.

In case B2 the offshore region is defined as $x_0 \leq x < x_k = 5$. One simulation is performed with the parameters $\Delta x = \Delta t = 0.1$, $a_0 = 0.2$ and $\lambda = 1$. In figure 5.1 the numerical solution of η is compared to the solution obtained by BMEP for three different times, $t = 1, 4, 7$.
The difference between the two outputs is introduced when producing the initial condition for BMEP. The difference does not grow over time and are of a constant order of magnitude $\mathcal{O}(10^{-7})$.

5.1.2 Refinement study

A refinement study was performed for two bathymetries to determine the coarsest grid resolution that yields a converged run-up height. The study was done for the two extrema of h_1, i.e. $h_1 = 0, 1$. In the case of $h_1 = 0$ the incline was set to $\alpha = 0.017$ which is the lowest degree of incline in this thesis. The results of $h_1 = 1$ is seen in figure 5.2 with corresponding ratio values in table 5.3. We observe that the grid resolution increases for smaller λ. The same is observed for the bathymetry with $h_1 = 0$ in figure 5.3. The grid resolution must however be much higher to reach a converged run-up height for this bathymetry.

Table 5.1: L^∞ and L^2 error for different values of Δx together with convergence rate for final refinement. Bathymetry is of constant depth.

	η		u	
Δx	L^∞	L^2	L^∞	L^2
$1.562{\cdot}10^{-1}$	$2.151{\cdot}10^{-2}$	$1.113{\cdot}10^{-3}$	$2.147{\cdot}10^{-2}$	$1.128{\cdot}10^{-3}$
$7.812{\cdot}10^{-2}$	$5.069{\cdot}10^{-3}$	$2.722{\cdot}10^{-4}$	$5.137{\cdot}10^{-3}$	$2.738{\cdot}10^{-4}$
$3.906{\cdot}10^{-2}$	$1.281{\cdot}10^{-3}$	$6.834{\cdot}10^{-5}$	$1.287{\cdot}10^{-3}$	$6.858{\cdot}10^{-5}$
$1.953{\cdot}10^{-2}$	$3.217{\cdot}10^{-4}$	$1.715{\cdot}10^{-5}$	$3.223{\cdot}10^{-4}$	$1.718{\cdot}10^{-5}$
Convergence	1.99285	1.99444	1.99728	1.99731

Case B1; λ=1.1, a_0=0.5, dt/dx=0.8

Table 5.2: L^∞ and L^2 error for different values of Δx together with convergence rate for final refinement. Bathymetry is of constant depth.

	η		u	
Δx	L^∞	L^2	L^∞	L^2
$1.562{\cdot}10^{-1}$	$2.631{\cdot}10^{-2}$	$1.403{\cdot}10^{-3}$	$2.776{\cdot}10^{-2}$	$1.400{\cdot}10^{-3}$
$7.812{\cdot}10^{-2}$	$6.645{\cdot}10^{-3}$	$3.527{\cdot}10^{-4}$	$6.652{\cdot}10^{-3}$	$3.546{\cdot}10^{-4}$
$3.906{\cdot}10^{-2}$	$1.666{\cdot}10^{-3}$	$8.883{\cdot}10^{-5}$	$1.676{\cdot}10^{-3}$	$8.921{\cdot}10^{-5}$
$1.953{\cdot}10^{-2}$	$4.189{\cdot}10^{-4}$	$2.232{\cdot}10^{-5}$	$4.197{\cdot}10^{-4}$	$2.236{\cdot}10^{-5}$
Convergence	1.99163	1.99248	1.99723	1.99595

Case B1; λ=1.1, a_0=0.5, dt/dx=0.5

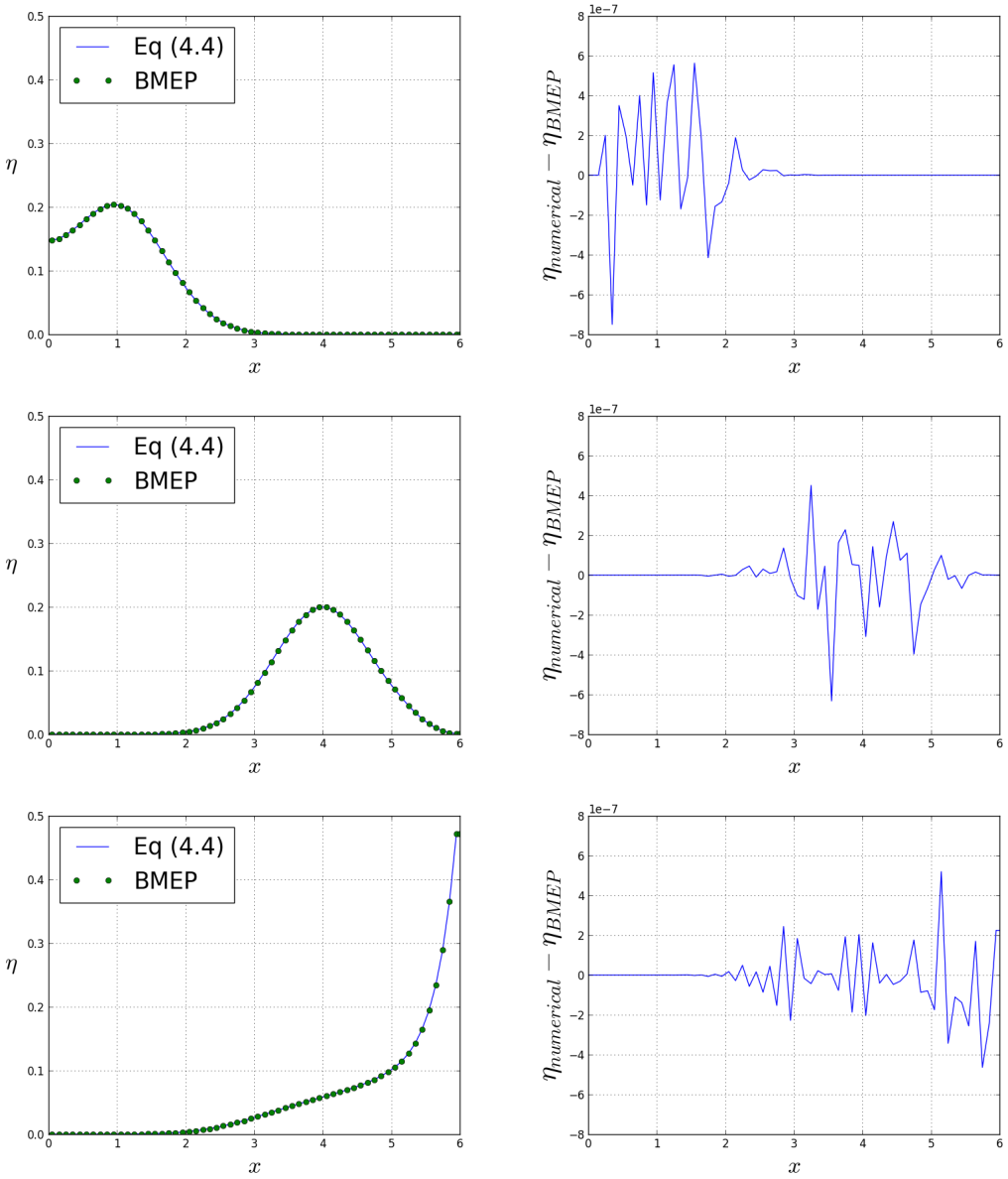

Figure 5.1: Comparing numerical solution with solution obtain with BMEP for $t = 1, 4, 7$. Left side: comparing values of η, right side: Difference between solvers.

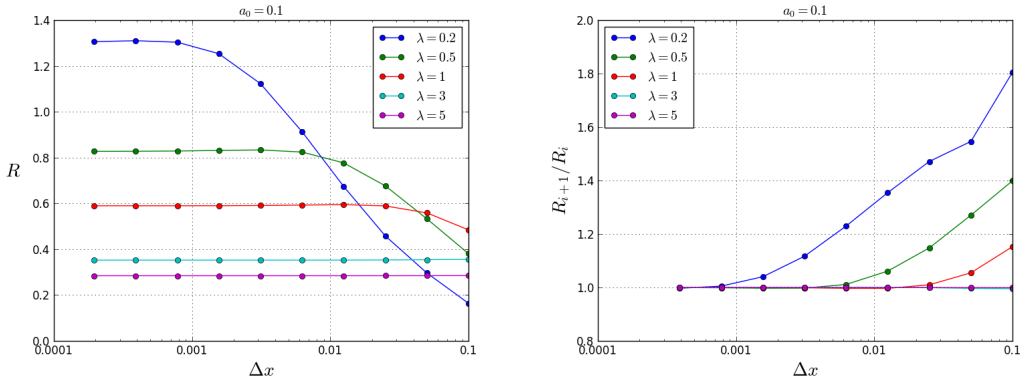

Figure 5.2: Run-up height for different wavelengths as a function of Δx. The right image is the run-up height ratio for two consecutive values of Δx. Bathymetry parameters; $h_1 = 1$.

Table 5.3: $R(\Delta x_{i+1})/R(\Delta x_i)$ for different λ corresponding to figure 5.2.

Δx_i	$\lambda = 0.2$	$\lambda = 0.5$	$\lambda = 1$	$\lambda = 3$	$\lambda = 5$
0.10000	1.80516	1.39901	1.15252	0.99516	0.99908
0.05000	1.54614	1.27016	1.05459	0.99643	0.99935
0.02500	1.47115	1.14781	1.00983	0.99908	0.99981
0.01250	1.35432	1.06098	0.99647	0.99962	0.99996
0.00625	1.22958	1.01118	0.99666	0.99990	0.99999
0.00313	1.11661	0.99734	0.99867	0.99998	1.00000
0.00156	1.04006	0.99700	0.99958	0.99999	1.00000
0.00078	1.00491	0.99874	0.99988	1.00000	1.00000
0.00039	0.99688	0.99960	0.99997	1.00000	1.00000
0.00020	-	-	-	-	-

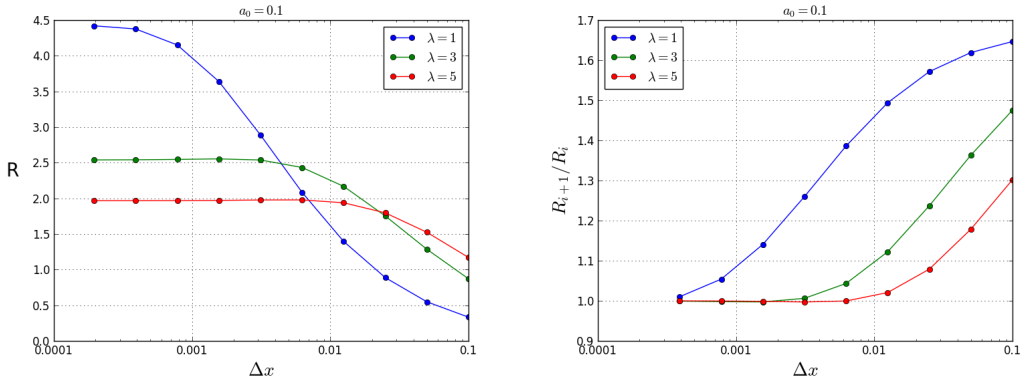

Figure 5.3: Run-up height for different wavelengths as a function of Δx. The right image is the run-up height ratio between two consecutive values of Δx. Bathymetry parameters; $h_1 = 1$, $\alpha \approx 0.017$.

Table 5.4: $R(\Delta x_{i+1})/R(\Delta x_i)$ for selected λ corresponding to figure 5.3.

Δx_i	$\lambda = 1$	$\lambda = 3$	$\lambda = 5$
0.10000	1.64661	1.47546	1.30204
0.05000	1.61912	1.36322	1.17859
0.02500	1.57151	1.23690	1.07891
0.01250	1.49400	1.12227	1.02059
0.00625	1.38605	1.04323	0.99953
0.00313	1.25989	1.00613	0.99709
0.00156	1.14069	0.99718	0.99857
0.00078	1.05409	0.99786	0.99952
0.00039	1.01011	0.99918	0.99986
0.00020	-	-	-

5.2 LSW - Phase plane solver

The numerical scheme for equation (4.6) is second order accurate. The incoming wave solution (3.6) yields a boundary condition $b_0 = 2a_0 ike^{-\frac{ik\Delta x}{2}}$ from (4.7). This boundary condition applies for all test cases.

5.2.1 Test results

For case B1, the test was performed with wave parameters $\lambda = 0.4$ and $a_0 = 0.2$. The results are displayed in table 5.5 and we observe that the convergence rate is quadratic.

For case B2, the offshore region is bounded by $0 = x_0 \leq x < x_k = 2$. Tests was performed with wave parameters $\lambda = 0.4, 1.1$ and $a_0 = 0.2, 0.3$ respectively. The results are displayed in tables 5.6 and 5.7. Quadratic convergence is obtained in both cases.

5.2.2 Refinement study

A refinement study was performed for the same two bathymetries as the time dependent solver, $h_1 = 0, 1$ with $\alpha = 0.017$ when $h_1 = 0$. Results are depicted in figures 5.4 and 5.5 with corresponding run-up ratio values in tables 5.8 and 5.9 respectively.

Table 5.5: L^∞ and L^2 error of η for a constant depth bathymetry. Convergence rate is for the last refinement.

Δx	L^∞	L^2
$1.250{\cdot}10^{-2}$	$9.865{\cdot}10^{-3}$	$3.386{\cdot}10^{-3}$
$6.250{\cdot}10^{-3}$	$2.442{\cdot}10^{-3}$	$8.410{\cdot}10^{-4}$
$3.125{\cdot}10^{-3}$	$6.080{\cdot}10^{-4}$	$2.090{\cdot}10^{-4}$
$1.563{\cdot}10^{-3}$	$1.520{\cdot}10^{-4}$	$5.200{\cdot}10^{-5}$
$7.813{\cdot}10^{-4}$	$3.800{\cdot}10^{-5}$	$1.300{\cdot}10^{-5}$
Convergence rate	2.00401	2.00410

Case B1; λ=0.4, a_0=0.2

Table 5.6: L^∞ and L^2 error of η for a single inclined plane bathymetry. Convergence rate is for the last refinement.

Δx	L^∞	L^2
$1.500{\cdot}10^{-3}$	$1.546{\cdot}10^{-2}$	$1.921{\cdot}10^{-4}$
$7.500{\cdot}10^{-4}$	$4.067{\cdot}10^{-3}$	$4.774{\cdot}10^{-5}$
$3.750{\cdot}10^{-4}$	$1.043{\cdot}10^{-3}$	$1.188{\cdot}10^{-5}$
$1.875{\cdot}10^{-4}$	$2.641{\cdot}10^{-4}$	$2.964{\cdot}10^{-6}$
$9.375{\cdot}10^{-5}$	$6.646{\cdot}10^{-5}$	$7.400{\cdot}10^{-7}$
Convergence rate	1.99091	2.00215

Case B2; λ=0.4, a_0=0.2.

Table 5.7: L^∞ and L^2 error of η for a single inclined plane bathymetry. Convergence rate is for the last refinement.

Δx	L^∞	L^2
$1.500{\cdot}10^{-3}$	$3.772{\cdot}10^{-4}$	$1.744{\cdot}10^{-5}$
$7.500{\cdot}10^{-4}$	$9.496{\cdot}10^{-5}$	$4.351{\cdot}10^{-6}$
$3.750{\cdot}10^{-4}$	$2.382{\cdot}10^{-5}$	$1.086{\cdot}10^{-6}$
$1.875{\cdot}10^{-4}$	$5.966{\cdot}10^{-6}$	$2.714{\cdot}10^{-7}$
$9.375{\cdot}10^{-5}$	$1.493{\cdot}10^{-6}$	$6.771{\cdot}10^{-8}$
Convergence rate	1.99882	2.00326

Case B2; λ=1.1, a_0=0.3.

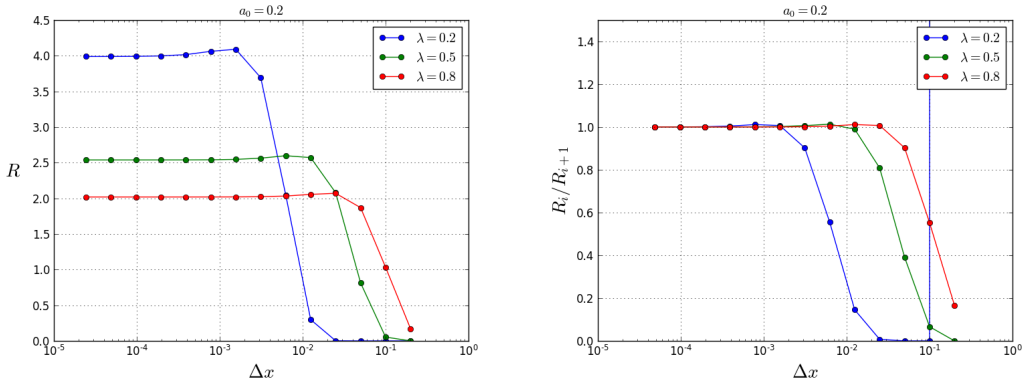

Figure 5.4: Refinement study for single inclined plane. Left figure displays run-up amplitude and right figure displays the run-up amplitude ratio.

Table 5.8: $R(\Delta x_i)/R(\Delta x_{i+1})$ for selected λ corresponding to figure 5.4.

Δx_i	$\lambda = 0.2$	$\lambda = 0.5$	$\lambda = 0.8$
0.20000	1696310	0.00000	0.16519
0.10000	0.00000	0.06634	0.55268
0.05000	0.00001	0.39090	0.90277
0.02500	0.00746	0.80870	1.00733
0.01250	0.14550	0.98987	1.01144
0.00625	0.55479	1.01335	1.00466
0.00313	0.90248	1.00672	1.00144
0.00156	1.00717	1.00222	1.00040
0.00078	1.01140	1.00063	1.00011
0.00039	1.00465	1.00017	1.00002
0.00020	1.00143	1.00004	1.00001
0.00010	1.00040	1.00001	1.00000
0.00005	1.00010	1.00000	1.00000
0.00003	-	-	-

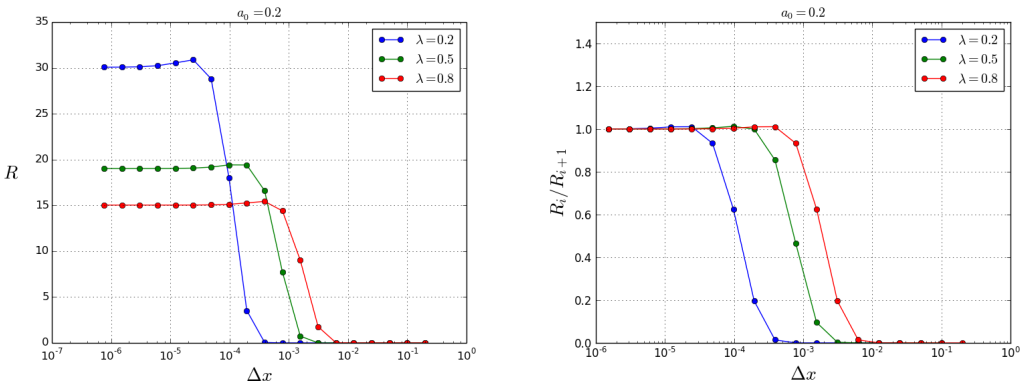

Figure 5.5: Refinement study for $h_1 = 0$ and $\alpha = 0.017$. Left figure displays run-up amplitude and right figure displays the run-up amplitude ratio.

Table 5.9: $R(\Delta x_i)/R(\Delta x_{i+1})$ for selected λ corresponding to figure 5.5.

Δx_i	$\lambda = 0.2$	$\lambda = 0.5$	$\lambda = 0.8$
0.006250	0.000000	0.000003	0.014081
0.003125	0.000000	0.003087	0.196058
0.001563	0.000000	0.095613	0.625593
0.000781	0.000060	0.464885	0.933032
0.000391	0.014084	0.855277	1.010806
0.000195	0.196084	0.999498	1.010218
0.000098	0.625604	1.012646	1.003901
0.000049	0.933036	1.005718	1.001172
0.000024	1.010805	1.001829	1.000320
0.000012	1.010220	1.000511	1.000082
0.000006	1.003896	1.000137	1.000023
0.000003	1.001173	1.000036	1.000005
0.000002	1.000322	1.000000	1.000000
0.000001	-	-	-

5.2.3 Run-up height for single inclined plane

For illustrative purposes we include the numerical solution to the run-up height as a function of the wavelength and compare it to the exact solution (3.12) and the approximate solution (3.14).

From figure 5.6 we see a good compliance between the numerical solver (4.6) and the exact solution (3.12). We take notice of the stationary infliction points along the curve.

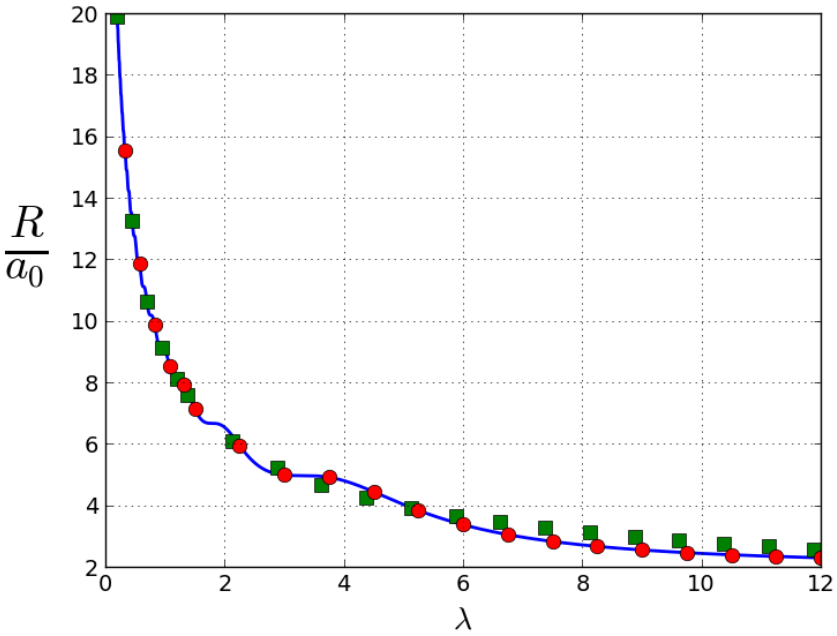

Figure 5.6: Relative runup amplitude as a function of the initial wave length. Solid line represents numerical solution (4.6), □ is approximation (3.14) and ∘ is exact solution (3.12).

5.3 GeoClaw

5.3.1 Refinement study

Two refinement studies were performed, one with $h_1 = 1$ (figure 5.7) and one with parameters $h_1 = 0$ and $\alpha = 0.017$ (figure 5.8). The CFL number was set to 0.7 for both studies.

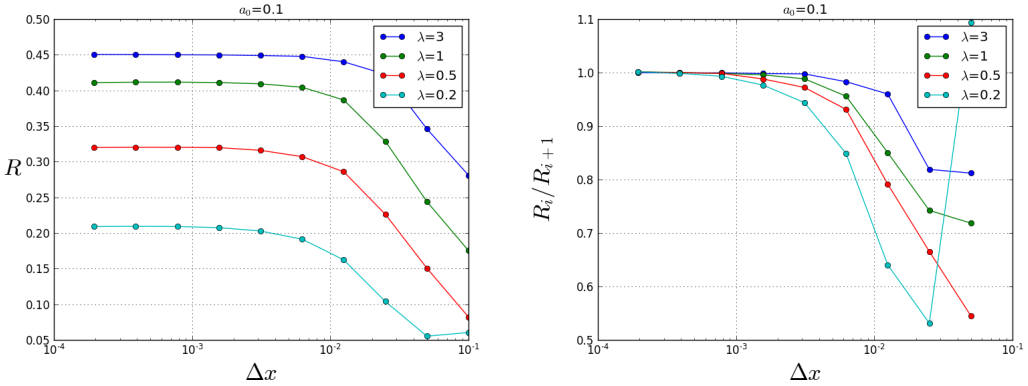

Figure 5.7: Left: Runup amplitude for various Δx on a single inclined plane. Right: Runup ratio. The x-axis is scaled logarithmic for illustration purposes.

Table 5.10: Values of R_i/R_{i+1} for different λ.

Δx	$\lambda = 0.2$	$\lambda = 0.5$	$\lambda = 1$	$\lambda = 3$
0.10000	0.81194	0.71843	0.54489	1.09322
0.05000	0.81893	0.74221	0.66549	0.53122
0.02500	0.96004	0.85039	0.79156	0.64052
0.01250	0.98296	0.95585	0.93106	0.84860
0.00625	0.99746	0.98832	0.97213	0.94374
0.00313	0.99815	0.99572	0.98810	0.97666
0.00156	0.99950	0.99843	0.99847	0.99311
0.00078	0.99927	1.00014	0.99989	0.99853
0.00039	0.99975	1.00146	1.00100	1.00152
0.00020	-	-	-	-

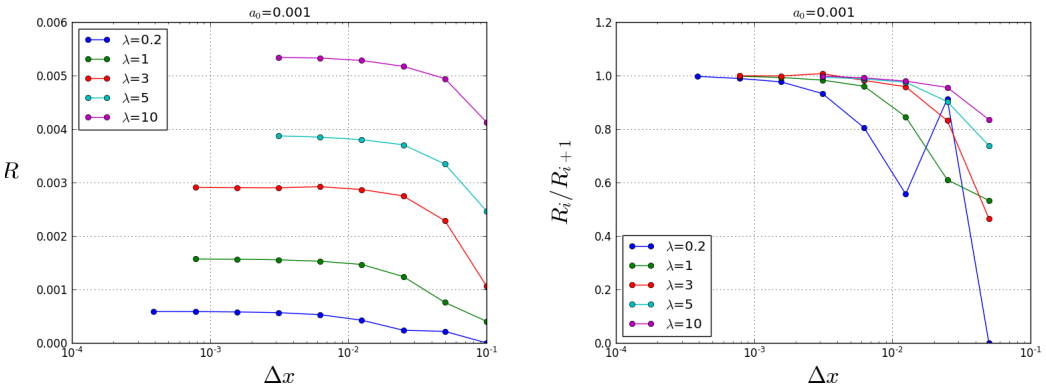

Figure 5.8: Left: Runup amplitude for various Δx with $h_1 = 0$ and $\alpha = 0.017$. Right: Runup ratio. The x-axis is scaled logarithmic for illustration purposes.

Table 5.11: Values of R_i/R_{i+1} for different λ.

Δx	$\lambda = 0.2$	$\lambda = 1$	$\lambda = 3$	$\lambda = 5$	$\lambda = 10$
0.10000	0.00000	0.53302	0.46582	0.73780	0.83533
0.05000	0.91268	0.61012	0.83141	0.90261	0.95565
0.02500	0.55703	0.84596	0.95828	0.97511	0.97915
0.01250	0.80492	0.96012	0.98183	0.98736	0.99143
0.00625	0.93260	0.98308	1.00724	0.99406	0.99808
0.00313	0.97664	0.99295	0.99861	-	-
0.00156	0.98909	0.99750	0.99909	-	-
0.00078	0.99703	-	-	-	-
0.00039	-	-	-	-	-

Chapter 6

Reflection

Wave reflection in an inhomogeneous medium is a well known phenomena but to the authors knowledge there is not much published literature on the subject from a water wave run-up point of view. Pedersen discusses the issue in the appendix of [13] and a linear relation between the reflected wave amplitude and the incident wavelength is presented. However, the study was done only for a single inclined plane bathymetry with parabolic cross-sections. The relation should still have some validity in the case of a rectangular cross-section but an investigation needs to be made and inclusion of a composite slope is of essence to determine the effects reflection might have on the run-up height in the general case. Effects of smoothing the discontinuous vertex connecting the slope to the constant depth region is also investigated as the topic often is avoided in published literature as studies are performed on either a smoothed bottom profile or a piecewise linear profile and not both.

6.1 Method

The results are obtained by simulating an incident wave traveling from the offshore region of constant depth to the near-shore region with a slope (see Fig. B.1). The two regions are connected by a sharp vertex at $x = x_k$. The simulations are

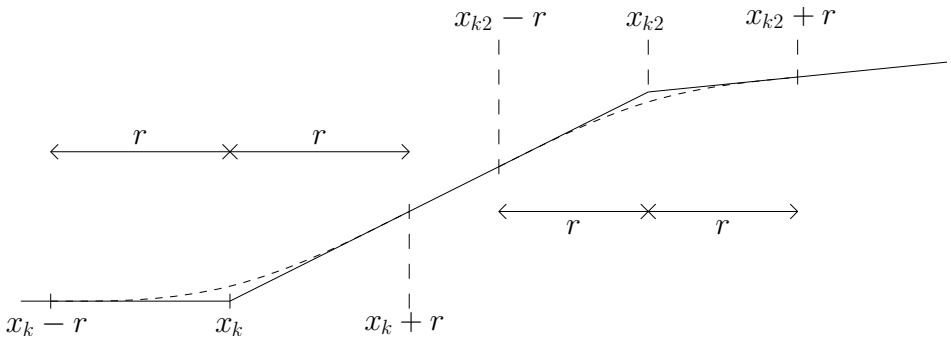

Figure 6.1: A sketch of the composite slope bathymetry consisting of two inclined planes. The dashed line illustrates the "smoothing" function.

performed for two different near-shore regions with $h_1 = 1, 0.9$ and $\alpha = 0.017$. The bathymetry with $h_1 = 1$ is effectively consisting of a single inclined plane. The two planes in the composite slope is joined by a sharp vertex at $x = x_{k2}$. For the numerical simulations we introduce a parameter r (see Fig. 6.1) which defines a horizontal length in each direction of x_k. In the area confined by $x_k - r \leq x \leq x_k + r$, we employ a smooth transition between the two regions by means of describing the bottom profile as a third order polynomial. The same will be done to smooth the transition between the two slope segments connected at x_{k2}.

The simulated wave have an initial wave shape described in (3.21) as $\eta(x, 0) = a_0 \operatorname{sech}^2(kx)$ where the wavenumber k is described in (3.23) as a function of the wavelength λ. It is important that the incident wave is unaffected by the near-shore bathymetry and to achieve this the offshore region must be of minimum length $x_k - x_0 \leq \lambda$. Furthermore, the time period t_p in which the simulation is performed is always of sufficient length to allow the entire transmitted wave to pass $x = x_k$ and in the case $h_1 = 0.9$, $x = x_{k2}$.

A parameter used in the results is the maximum reflected amplitude and it is defined as

$$a_R = \frac{max(\eta(x,t))}{a_0}\,, \qquad \text{for} \quad x \leq x_k - r \quad \text{and} \quad t = t_0\left(1 + \frac{r}{x_S}\right) \tag{6.1}$$

where t_0 is the simulation time in the case when $r = 0$.

6.2 Results

6.2.1 Single inclined plane

A section of the bottom profile is depicted in figure 6.2 with $r = 0, 0.5, 1$. The vertex connecting the offshore region and the near-shore region is located at $x_k = 4.0$.

The surface elevation of a wave with initial amplitude $a_0 = 0.1$ and wavelength $\lambda = 0.5$ is depicted in figure 6.3. The time of depiction, t_0, is when the maximum height of the transmitted wave was located at $x = x_S - 0.5\lambda$. We observe that the incident wave shape is transformed into a similar wave shape plus a long shelf as the wave passes the point $x_k - r$. The transmitted wave has a decreased wavelength and an increased wave height compared to the initial wave. The wave height of the transmitted wave is slightly higher in the case of $r = 1$. The shape of the reflected wave is apparently dependent on r which is emphasized in figure 6.4. When $r = 0$ the reflected wave has a clearly defined wave front with the shelf as a trailing current. The amplitude of the wavefront is large compared to the case with $r = 1$. When the bottom profile is smoothed with $r = 1$ the reflected wave height is constantly decreasing away from $x_k - r$. In figure 6.5 we see the surface elevation at x_k as a function of time, $\eta(x_k, t)$. $t = 0$ is the time when the maximum wave height passed x_k. An increased wave height peak for higher values of r is observed. Since these waves will have propagated a length r over a decreasing depth this is expected. After the transmitted wave has passed x_k we observe a constant wave height for the time period depicted. This indicates that the reflection current is stationary from a linear slope. The reflected wave height

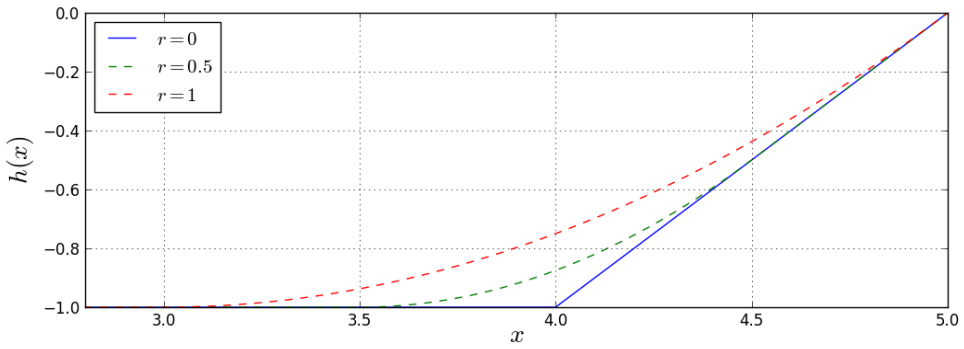

Figure 6.2: Bottom profile with a single inclined plane starting at $x_k = 4.0$ with $r = 0, 0.5, 1$.

will remain constant until we get reflection from the shoreline.

Inspired by Pedersen [13] we investigate the linear relation between the wavelength and a_R. From figure 6.6 we observe that the relation is linear for wavelengths $\lambda < L$. The maximum reflected amplitude increases as the wavelength increases. The difference of $a_R(r = 0)$ and $a_R(r = 1)$ is between $2.5\% - 3\%$. This is also the case for wavelength $\lambda > L$. The reduction of a_R for larger r could help explain the increase in the maximum wave height observed in figure 6.3 and 6.5. However, there have not been found an increase or decrease of the same magnitude in the run-up height when smoothing the vertex (see section 6.3). This could indicate that by smoothing the vertex the shape and amplitude of the reflected wave is altered, but the total reflection is not affected in the same way. Therefore an attempt to investigate the change in the total volume of the reflected wave V_{tot}, i.e. the sum of the area confined by the surface elevation and the unperturbed water surface.

This yielded no valuable information in this case. This might be caused by the difficulty of defining the area in which a continuous wave is confined.

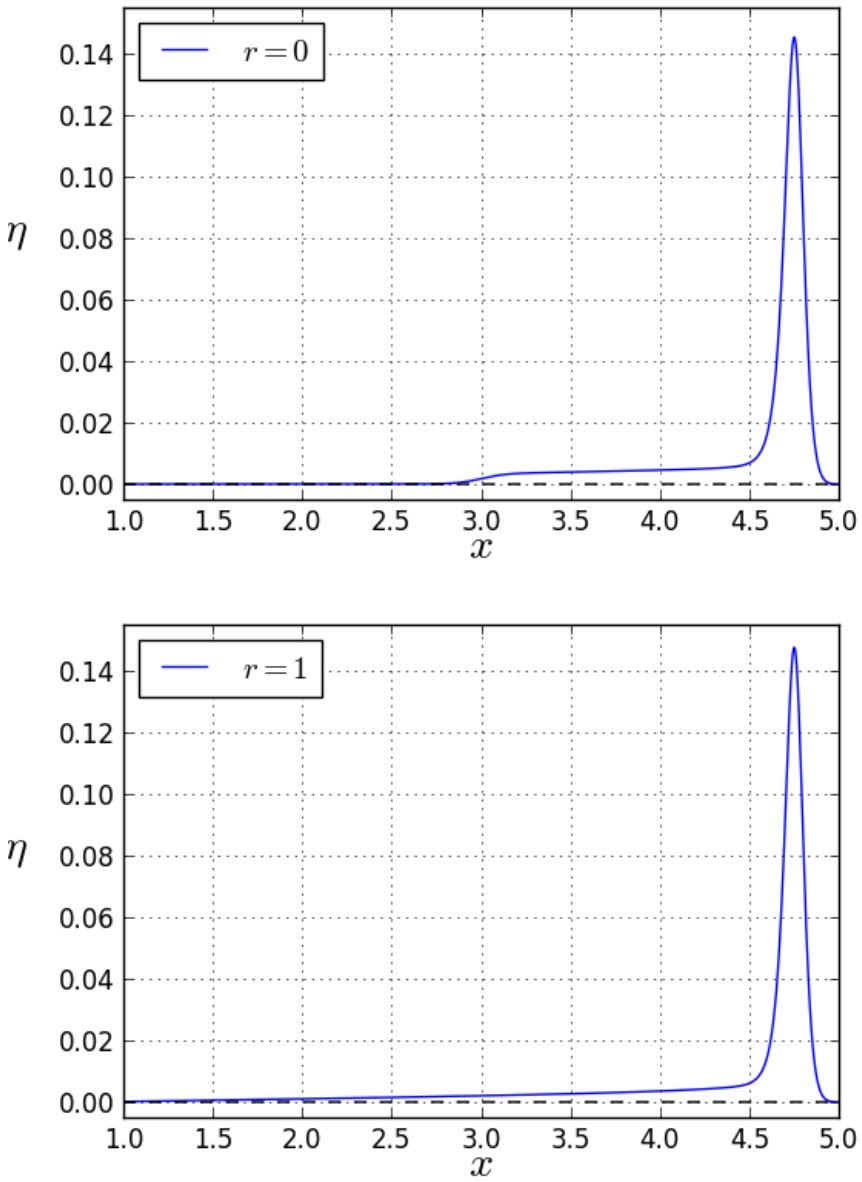

Figure 6.3: Linear surface elevation for traveling wave with initial $a_0 = 0.1$ and $\lambda = 0.5$. The dashed line marks the unperturbed surface. The top image has a discontinuous vertex at x_k whereas the bottom image has a smoothed bottom profile with $r = 1$.

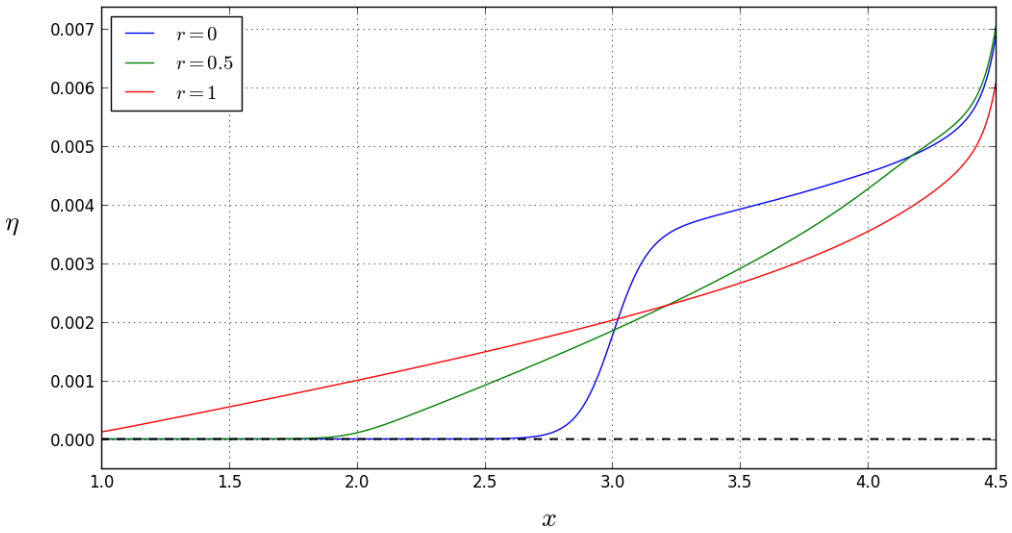

Figure 6.4: Cropped image of figure 6.3. The surface elevation with $r = 0.5$ is included.

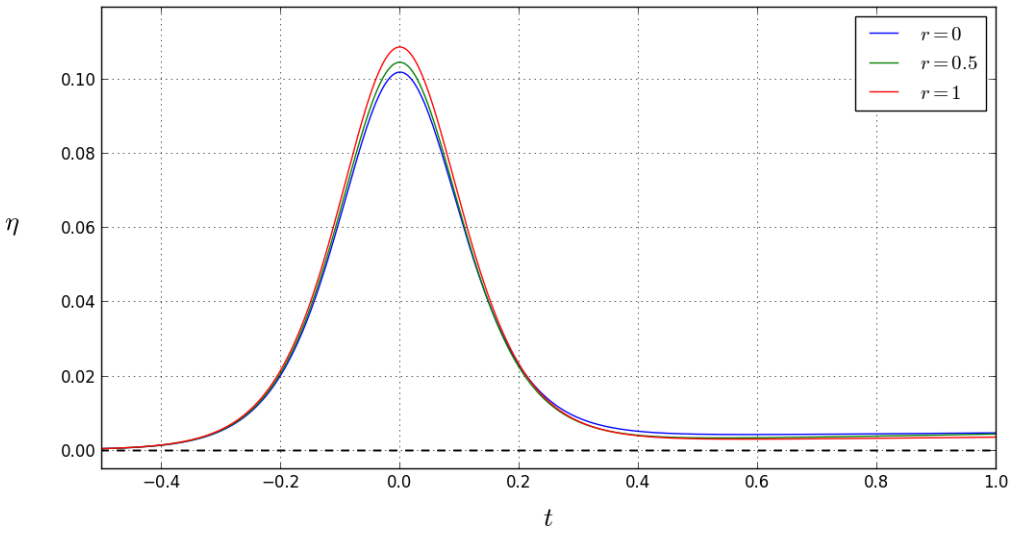

Figure 6.5: A time plot of the surface elevation at $x = x_k$. $t = 0$ is the time when the maximum wave height passed x_k.

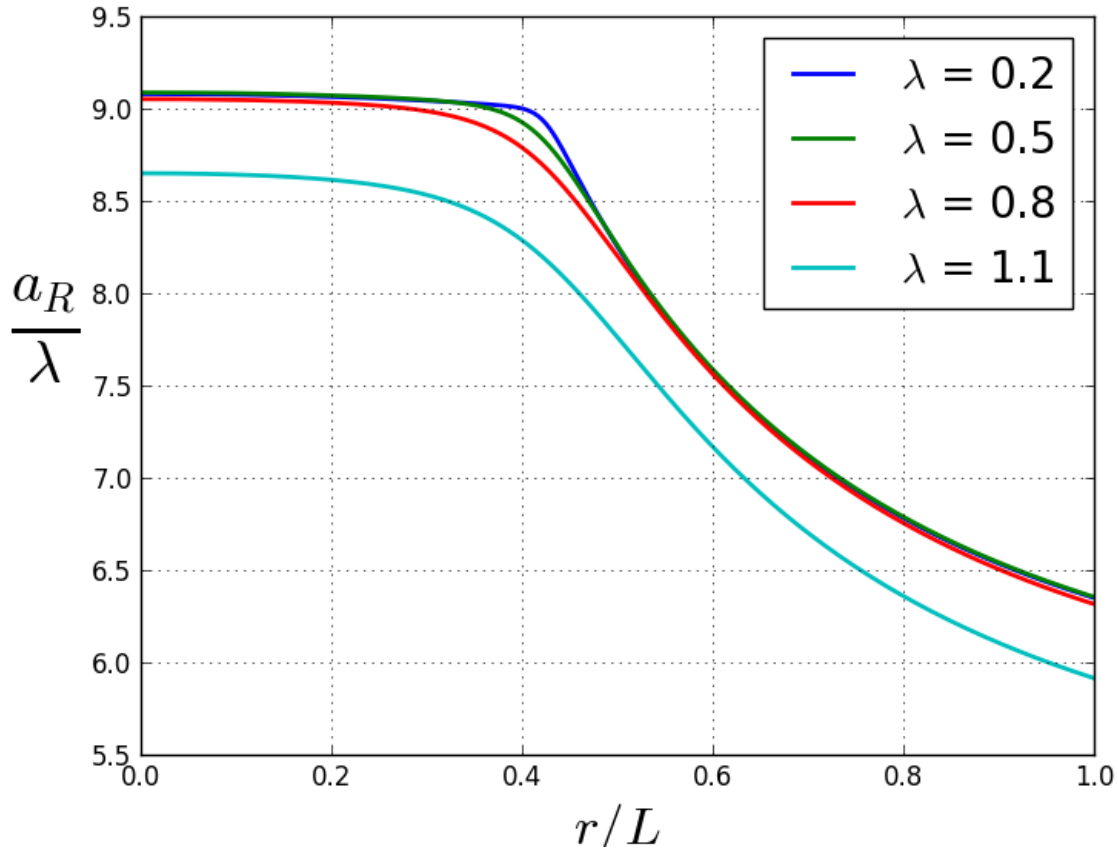

Figure 6.6: Maximum reflection amplitude per wave length in percent for LSW.

6.2.2 Composite slope

A section of the bottom profile is depicted in figure 6.7 and we see that the vertex separating the offshore region and the near-shore region is located at $x_k = 6.0$ and the vertex connecting the two slope segments is located at $x_{k2} = 6.9$ with $h_1 = 0.9$. For this bottom profile the range of r values are limited to $0 \leq r \leq 0.45$.

The surface elevation of the wave is depicted in figure 6.8 for $r = 0$ and $r = 0.45$. In the case with $r = 0$ we observe a reflected wave which is clearly separated from the transmitted wave and it forms a confined wave shape. It's maximum height seems to stem from the vertex connecting the two slope segments at x_{k2}. We also notice the dip, i.e. the trough, trailing after the transmitted wave. For the case of $r = 0.45$ the reflected wave is elongated and stretched over a large. The wave reflection is distributed over the whole slope. In the cropped view of the reflected wave (see Fig. 6.9) it is observed that the front of the reflected wave is of the same shape as for the single inclined plane. In the case of $r = 0$ there is also a trough trailing the reflected wave. Both vertexes in this bathymetry seems to induce a distinct reflected wavefront. But when a vertex connecting a concave slope creates a wavefront with a trailing shelf, the vertex connecting a convex slope creates a wavefront which severs the shelf connecting it to the transmitted wave. When looking at the surface elevation at x_k for a time period we see that the vertex at x_{k2} creates the maximum height of the reflected wave. When the vertex is smoothed with $r = 0.45$ the wave reflection is constantly decreasing. It may seem to go towards zero but there will remain a small reflection until the wave is reflected at the shoreline. The small value is due the low incline angle of the second slope segment.

The linear relation between a_R and λ investigated and the results are depicted

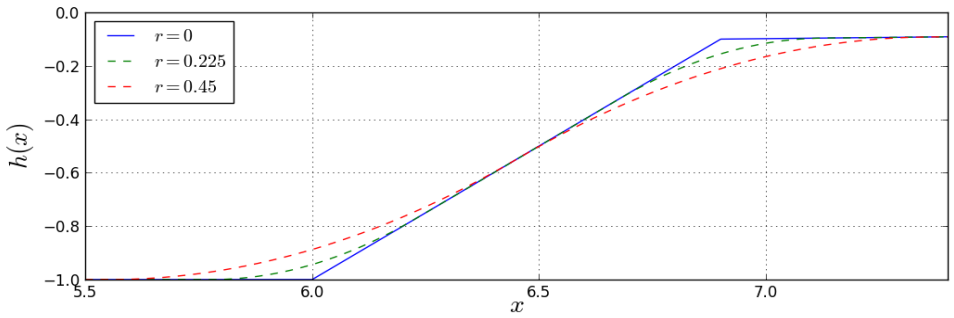

Figure 6.7: A composite slope starting at $x_k = 6.0$, $h_1 = 0.9$ and $\alpha = 0.017$ with $r = 0, 0.225, 0.45$.

in figure 6.11. There is a big difference in a_R/λ for $r = 0$. The ratio seems to converge as r increases.

In this case the reflected wave is clearly separated from the transmitted wave, but the reflected volume, V_{tot}, showed almost no differences for $r = 0$ and $r = 45$.

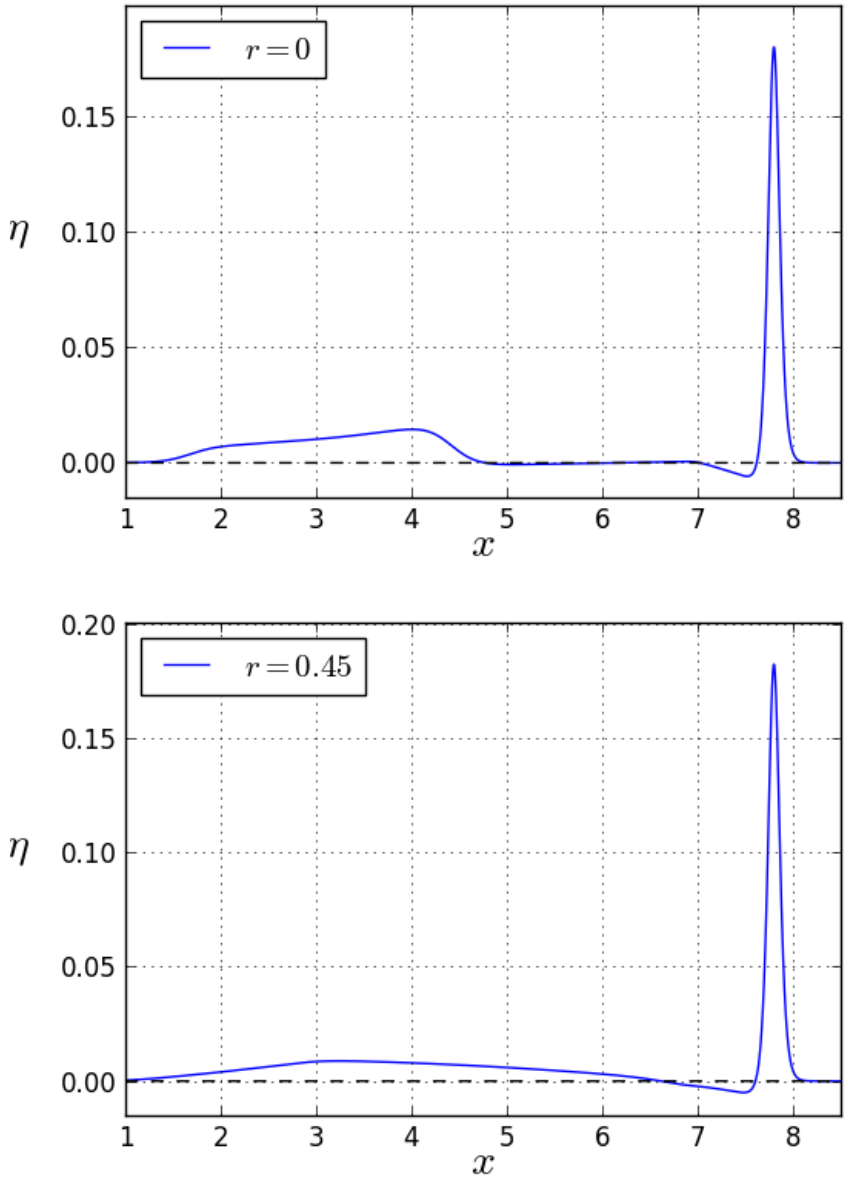

Figure 6.8: Linear surface elevation for wave with initial $a_0 = 0.1$ and $\lambda 1.0$ at some time after the entire transmitted wave had passed x_{k2}. The dashed line marks the unperturbed surface. Top: Surface elevation when $r = 0$, bottom: $r = 0.45$.

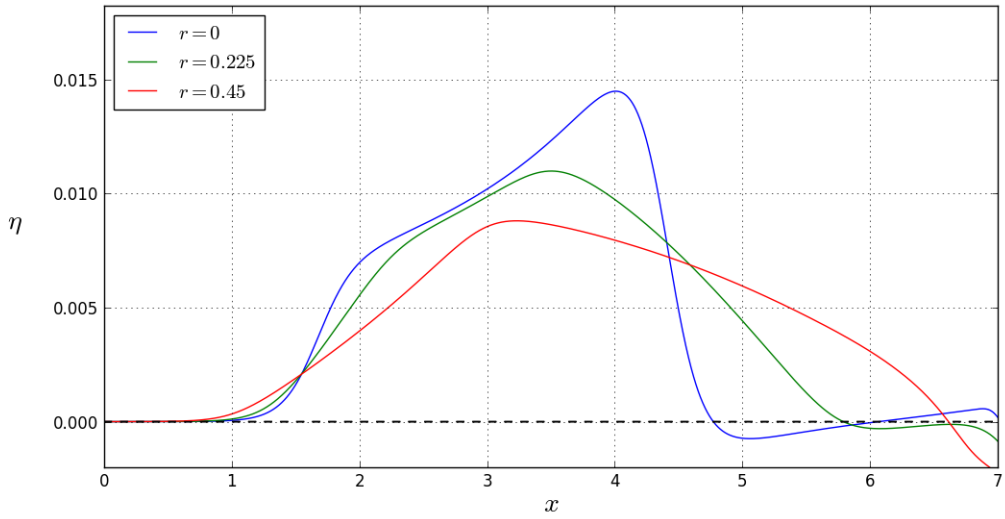

Figure 6.9: Cropped view comparing the reflected waves for $r = 0, 0.225, 0.45$.

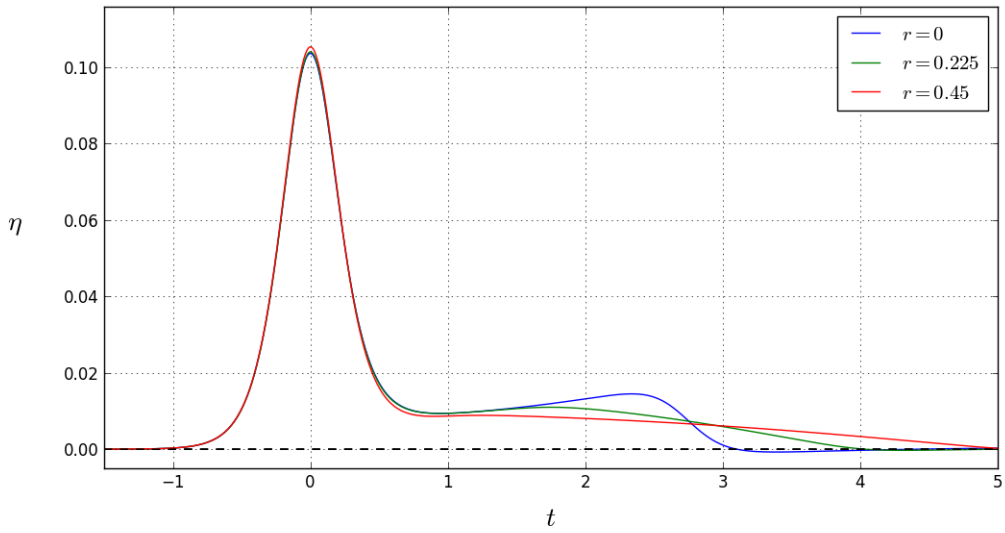

Figure 6.10: A time plot of the surface elevation at $x = x_k$. $t = 0$ is the time when the maximum wave height passed x_k.

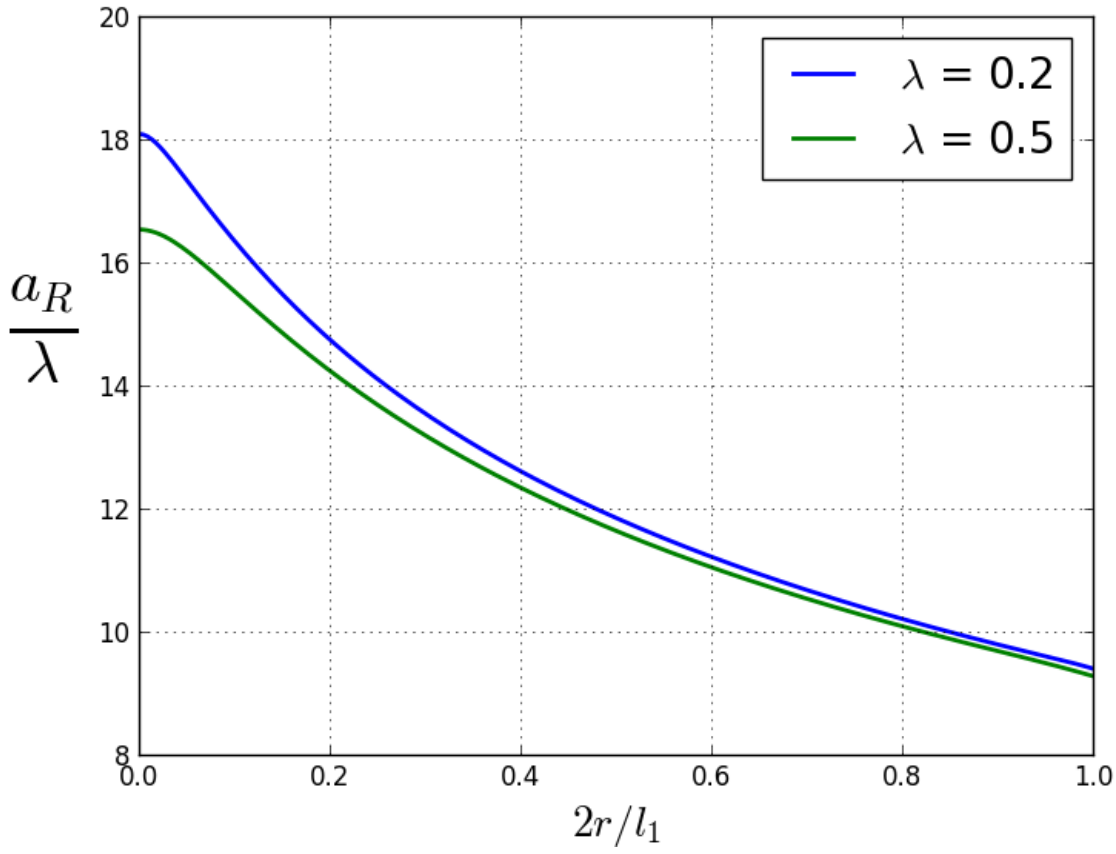

Figure 6.11: Maximum reflection amplitude per wave length in percent for LSW.

6.3 A note about the effects of r

The run-up height have been calculated for a the two bathymetries for selected values of r. For linear waves the run-up height is only affected by $\sim \pm 1\%$ even though a_R can reach several percent of a_0. This indicates two things. The first is that smoothing of the vertexes connecting the different slope segments is of minor consequence for the linear run-up height and does not need to be included in further calculations. The other is neither a_R is probably not the best estimate of which effects the vertexes have on the run-up height. One solution might be that the smooth slope increases the length of water depth shallower than 1 and thus reducing the average incline angle of the slope. In the non-linear case the run-up height is also only affected by $\sim 1\%$ in the single inclined plane case. In the composite slope case, the run-up height can vary as much as $\sim 5\%$. This is most likely due that a smoothing of the vertexes can induce breaking of waves that otherwise would not break. However, the results were not conclusive and further investigations should be made in all cases.

Chapter 7

Run-up Height

The run-up height of long waves are a well studied field and there are many publications of solutions and methods that can solve certain problems with satisfactory results. The main object in this chapter is to identify the crucial parameters that effects the run-up height. Periodic waves and single waves, both breaking and non-breaking, are simulated over various composite slope bathymetries to define important trends.

Some parameters are of special interest. Kânoğlu and Synolakis [7] reported that run-up height for non-breaking waves was affected only by the slope segment closest to the shoreline for values $h_1 \sim 0.5$. [22] presented results which suggested that non-breaking waves with high a_0, i.e. steep waves, would have increased run-up height compared to the ones with lower a_0. This is however only valid until the point where the waves break.

The breaking parameter introduced in (3.25) are used for guidance when it comes to choosing which values of λ, a_0 and α to investigate.

The bottom profile used in the numerical simulations is the composite slope illustrated in figure B.1. To ensure that the incoming wave is unaffected by the near-shore region the length of the offshore area is set to $d = x_k - x_0 = \lambda$, except in the section where the effects of the offshore length on the run-up height are reported. When solving the NLSW the CFL number is set to 0.7 as it was when

performing the refinement tests. However, for some of the simulations where bottom friction is neglected the simulations were performed with CFL= 0.5 to avoid crashing of the program.

A note must be made of the accuracy of the NLSW calculations. The discretization demanded for a converged run-up height found in chapter 5 is extremely time consuming. For waves with initial amplitude of $a_0 \geq 0.001$ the run-up height is found to be converged. For the waves with lower initial amplitude the accuracy is decreasing. Some results obtained with such low amplitudes are anyhow included in the results as they have some value in a quantitative way.

7.1 Linear periodic waves

The run-up height of linear periodic waves are calculated with Eq. (4.6) for a vast amount of parameter combinations. The crucial parameters that needed to be investigated was reported in chapter 3 to be the offshore wavelength λ, the height of the first slope segment h_1 and the incline angle of the second slope segment α.

The run-up heights increases as λ and α decreases (see Fig. 7.1) and for large values of λ and α the relative run-up height $R/a_0 \to 2$. Both observations are consistent with the exact solution (3.12) derived for a single inclined plane. We observe that the run-up height is not affect by the first slope segment for small values of h_1. When $h_1 = 0.5$ there are only minor changes in the run-height for certain values of λ and α but when $h_1 = 0.9$ these changes are noticeably enhanced. In figure 7.2 we observe that these changes are due the stationary infliction points we observed in figure 5.6 turning into extrema as h_1 increases. We notice that the infliction points are far less enhanced when $h_1 = 0$ than when $h_1 = 1$ for $\alpha = 0.017$. This difference is reduced when $\alpha \to 1$. The magnitude and frequency of the extrema increase with higher h_1 and lower α. We mention that the average value of the extrema is $R(h_1 = 0)$ even when $h_1 = 0.9$.

A cropped view of the smallest wavelengths and incline angles are depicted in figure 7.3. Here it is easier to observe that the run-up height rapidly increases when $\lambda \to 0$. When $h_1 = 0.9$ run-up height of short waves can be estimated based only on α with a maximum error of 10% at the extrema. When $h_1 = 0.999$ the magnitude of the extrema is double the run-up height $R(h_1 = 0)$ but the fluctuations are still centered around $R(h_1 = 0)$ (see Fig. 7.4).

The results shows that the linear run-up height can with good measure be estimated by the incline angle of the slope segment closest to the shoreline for $h_1 \leq 0.5$. This is consistent with what Kânoğlu and Synolakis [7] reported for a solitary wave.

We must also mention that even in the extreme case, i.e. $h_1 = 0.999$ and $\alpha = 0.017$, that the average values of the extrema are still close to $R(h_1 = 0)$. And for the waves with the highest run-up height, i.e. waves with short initial wavelengths, the run-up height can be determined with an error estimate of about 10%.

The occurrence of these extrema are reminiscent of results obtained by Pedersen [18]. However, his results stemmed from a run-up study of waves with an oblique angle of incident on a straight beach. Due to refraction of such waves it is possible that the experienced bottom profile will be more like a composite slope than a straight slope and thus result in a similar behavior. However, this is not further investigated and a thorough study needs to be performed before any conclusions can be drawn.

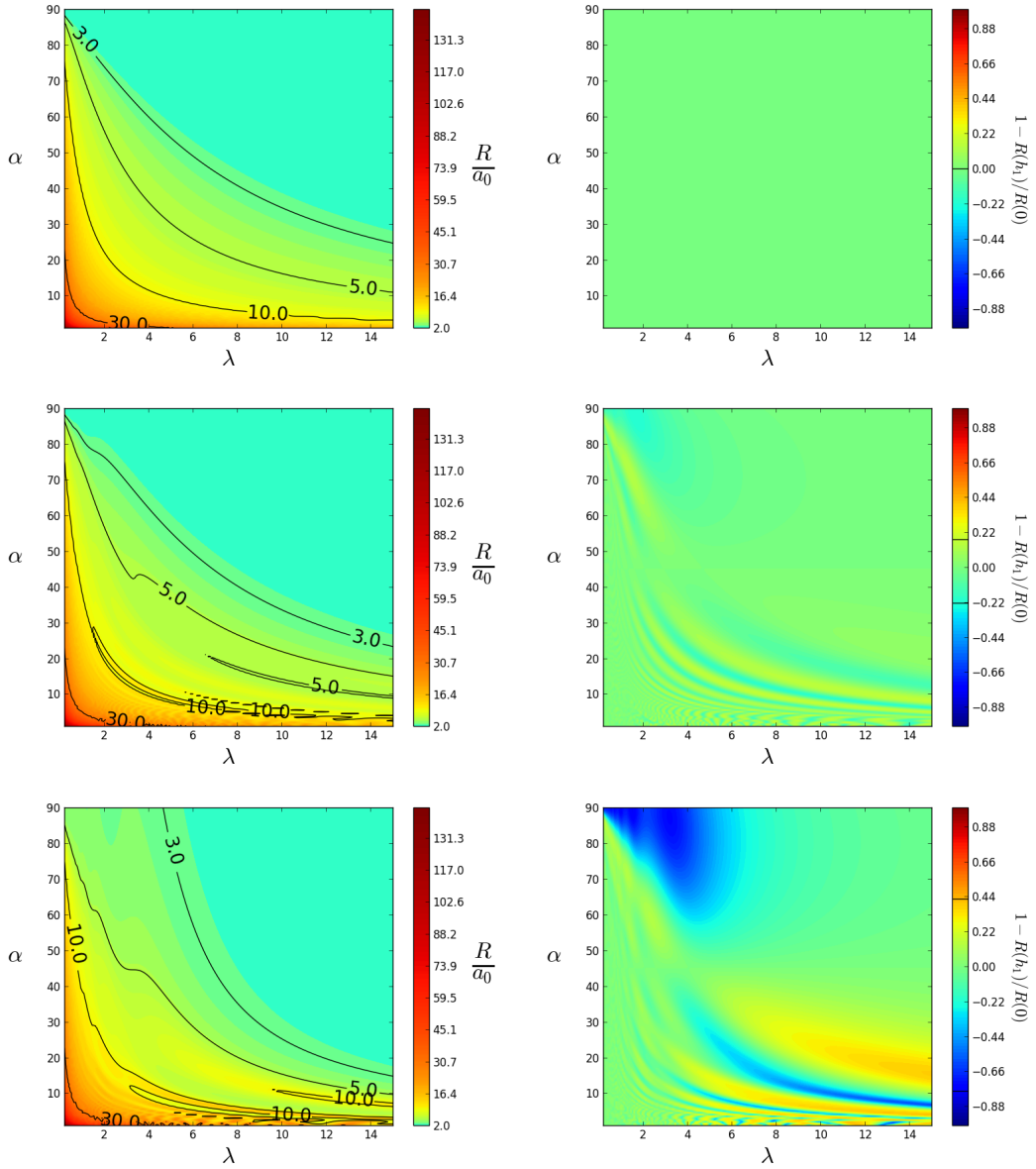

Figure 7.1: Left column: Contour plot of relative run-up amplitude, right column: Contour plot of the relative difference. Lines in the colorbar indicates maximum and minimum values in the figure. α is denoted in degrees for illustration purposes. Top row: $h_1 = 0.1$, middle row: $h_1 = 0.5$, bottom row: $h_1 = 0.9$

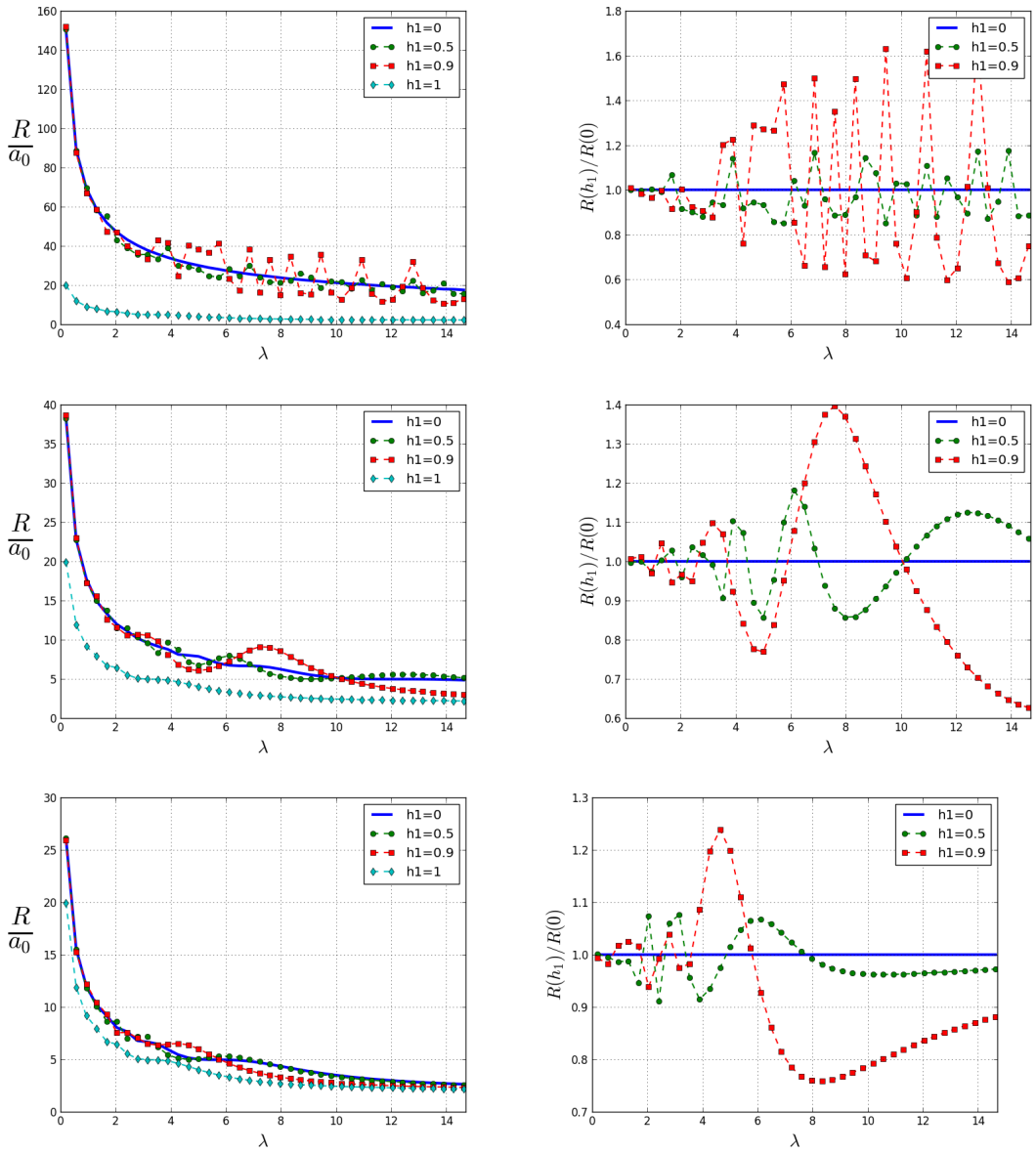

Figure 7.2: Left column: Relative run-up height for different α, right column: Run-up height ratio with $R(h_1 = 0)$ as comparison value. Top row: $\alpha = 0.017$, middle row: $\alpha = 0.27$, bottom row: $\alpha = 0.58$

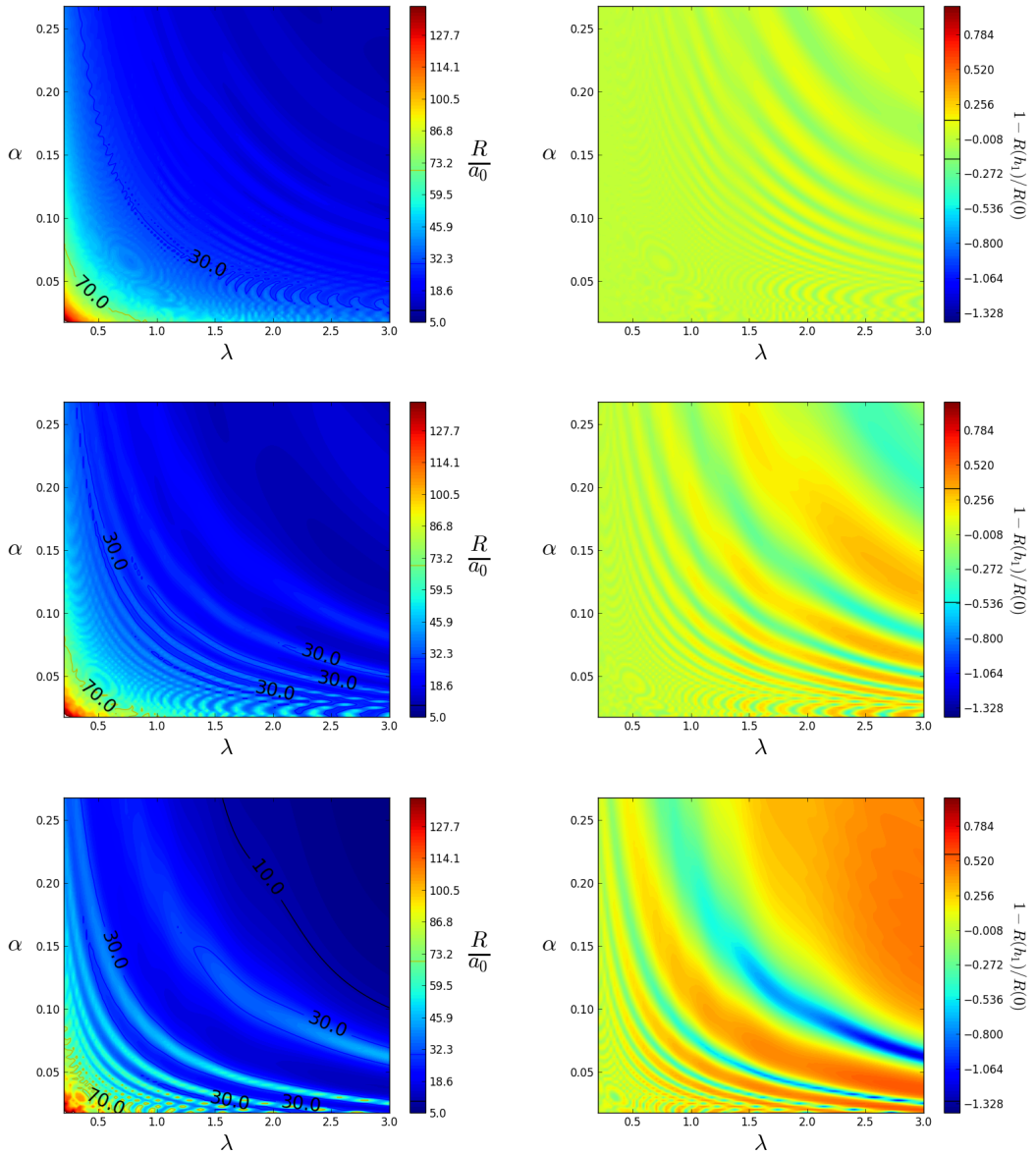

Figure 7.3: Left column: Contour plot of relative run-up amplitude, right column: Contour plot of the relative difference. Lines in the colorbar indicates maximum and minimum value of the difference. Top row: $h_1 = 0.9$, middle row: $h_1 = 0.99$, bottom row: $h_1 = 0.999$.

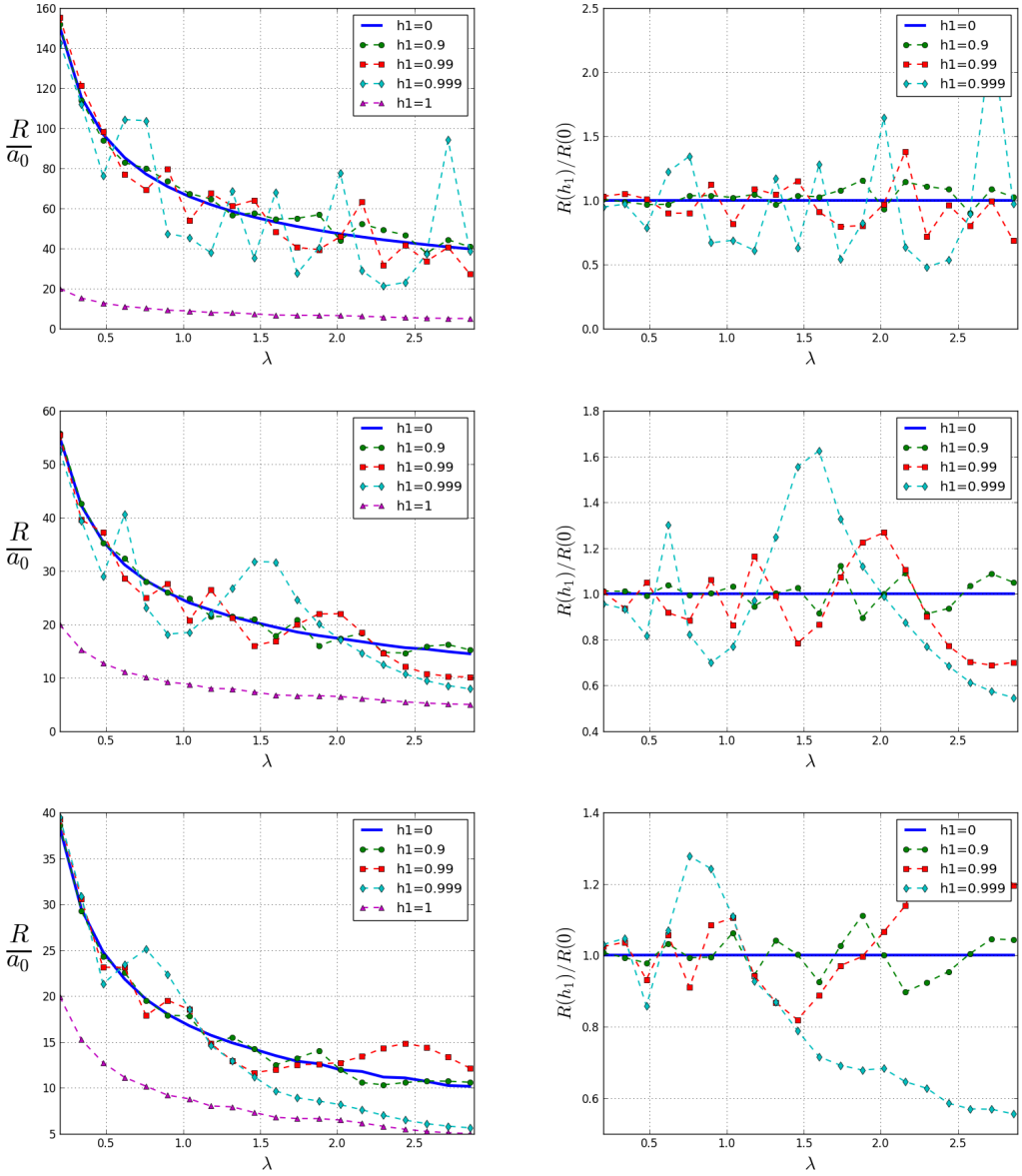

Figure 7.4: Left column: Relative run-up height for different α, right column: Run-up height ratio with $R(h_1 = 0)$ as comparison value. Top row: $\alpha = 0.017$, middle row: $\alpha = 0.27$, bottom row: $\alpha = 0.58$

7.2 Steepness effects on run-up height

The parameter d (see Fig. B.1) is the length which the center of the initial wave needs to travel before it reaches the near-shore region at $x = x_k$. The minimum distance to ensure that the initial wave is unaffected by the slope is $d = \lambda$. For non-linear waves the the phase speed increases with the wave height, meaning that for two points on the waves surface the highest point will travel with a greater speed than the lower one. This implies that the steepness of the wavefront at x_k will increase as d grows.

In figure 7.5 the relative run-up height as a function of d, where d is expressed as x_k/λ, is depicted for $a_0 = 0.01, 0.1, 1.0$ together with the LSW run-up height. The LSW run-up height is not affected by d since the equations are linear and non-dispersive. For the three cases of NLSW run-up height a change in d has a different effect on the wave depending on a_0. The run-up height of the wave with $a_0 = 0.01$ increases with d. The wave with $a_0 = 0.1$ increases at first but decreases when d becomes to large. The last, $a_0 = 1$, decreases it's run-up height for any increase of d. This implies that the run-up height increases with the steepness of the wavefront until the wave becomes so steep that it breaks. Upon breaking energy dissipates and momentum is lost and thus resulting in a lower run-up height. This is in compliance with the results of Synolakis [22].

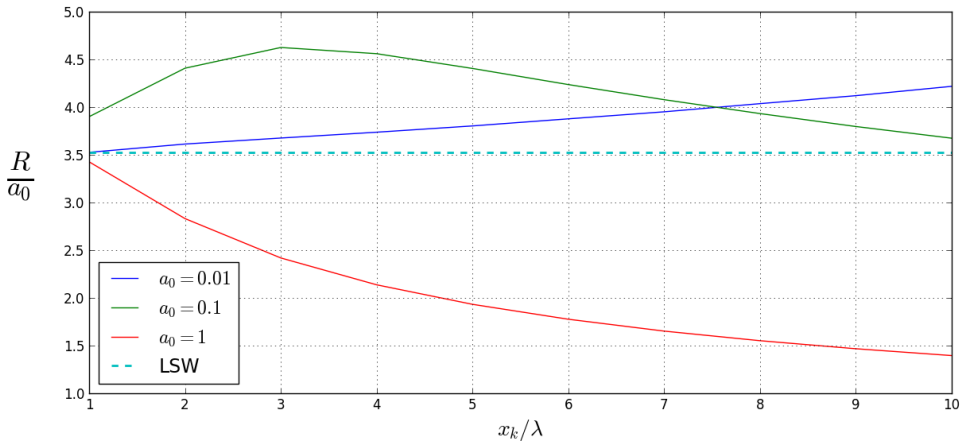

Figure 7.5: Run-up height as a function of d expressed as x_k/λ for $a_0/h_0 = 0.01, 0.1, 1$ and $\lambda = 3$.

7.3 Traveling waves

First we introduce some contour plots in figure 7.6. They depict the NLSW run-up height for a wave with initial amplitude $a_0 = 0.01$ on a bottom profile with $h_1 = 0.9$. This is included to highlight the difference in the run-up height for LSW and NLSW for waves with different steepness. In the top row we observe that the run-up height is higher when we neglect the bottom friction. The difference is quite noticeable. The difference in run-up height compared to LSW is apparent both with bottom friction and without. For both cases the run-up height is much less than the LSW run-up height for small wavelengths. This is due to waves with high ratios a_0/λ will break faster than the ones with a large ratio. We observe that the case without friction yields run-up heights that are closer to the LSW run-up height. But both NLSW solutions approaches the LSW solution when λ and α increases.

The NLSW run-up height as a function of h_1 is depicted for $\lambda = 3$ and $\alpha = 1^\circ$ for a sample of values of a_0 in figure 7.7. The LSW run-up height is included for comparison and we see that none of the NLSW values are close to this. It is also shown that the run-up height when neglecting the bottom friction is much larger than without. That none of the NLSW solutions are close to the LSW solution can be explained by the breaking parameter yielding a maximum initial amplitude of $a_0 = 0.00001$ to avoid reduction in the run-up height.

In figure 7.8 the NLSW run-up height is depicted for the same bathymetry but with $\lambda = 10$. The run-up height for small a_0 is much closer to the LSW solution. But for the larger amplitudes the reduction in run-up height is still apparent.

In the following two figures, 7.9 and 7.10, the incline angle of the second slope segment is increased to $\alpha = 5^\circ$. Now the solution is much closer to the LSW solution for most amplitudes where $\lambda = 10$. We do notice the run-up height for the waves with the two highest amplitudes, $a_0 = 0.1, 0.25$, have an increase in run-up height $h_1 \sim 0.9$ but decreases in both directions. The NLSW solution without bottom friction exceeds the LSW solution. For $\lambda = 3$ we observe the same trend.

In the last two figures, 7.11 and 7.12, it is hard to differentiate the run-up height for most values of a_0 in the case where $\lambda = 10$. In the case of $\lambda = 3$ there is still some distance to the LSW solution.

The run-up height for non-breaking seems unaffected by the first slope segment when $h_1 = 0.5$ which is what was presented by Synolakis [22]. For $\lambda = 3$ the run-up height is only changed by $\sim 3\%$ when $h_1 = 0.8$. For $\lambda = 10$ this is not the case as the run-up height have changed $\sim 5\%$ when $h_1 = 0.6$. The results

might differ somewhat due to the difference in wavelength and wave shape. The wavenumbers used in the results [22] was $k_{sol} = 0.027, 0.087$ which is the equivalent of $\lambda = 134, 42$ for the wave used here. Another difficulty when comparing with Synolakis is the scaling of the slope. The slope segment closest to the shoreline was scaled with the same scaling as used for the first slope segment here. Judging from the results presented here all waves of such low amplitudes would be similar to the LSW solution if $\alpha = 1$. The long waves used by Synolakis yields $R/a_0 \to 2$ which indicates that his waves are very long compared to the slope.

An important observation is that the run-up height for waves with a high initial amplitude also seems to go towards a constant run-up height as $h_1 \to 0$. A notice is taken that for certain parameter combinations such as $\lambda = 3$, $\alpha = 5$ and $a_0 = 0.01$ the run-up height is only changed by 0.2% between $h_1 = 0$ and $h_1 = 0.9$. This might indicate that wave breaking, just as the run-up height, is a phenomena which is decided by the parameters in the region where $h \to 0$. This is however not confirmed by these results.

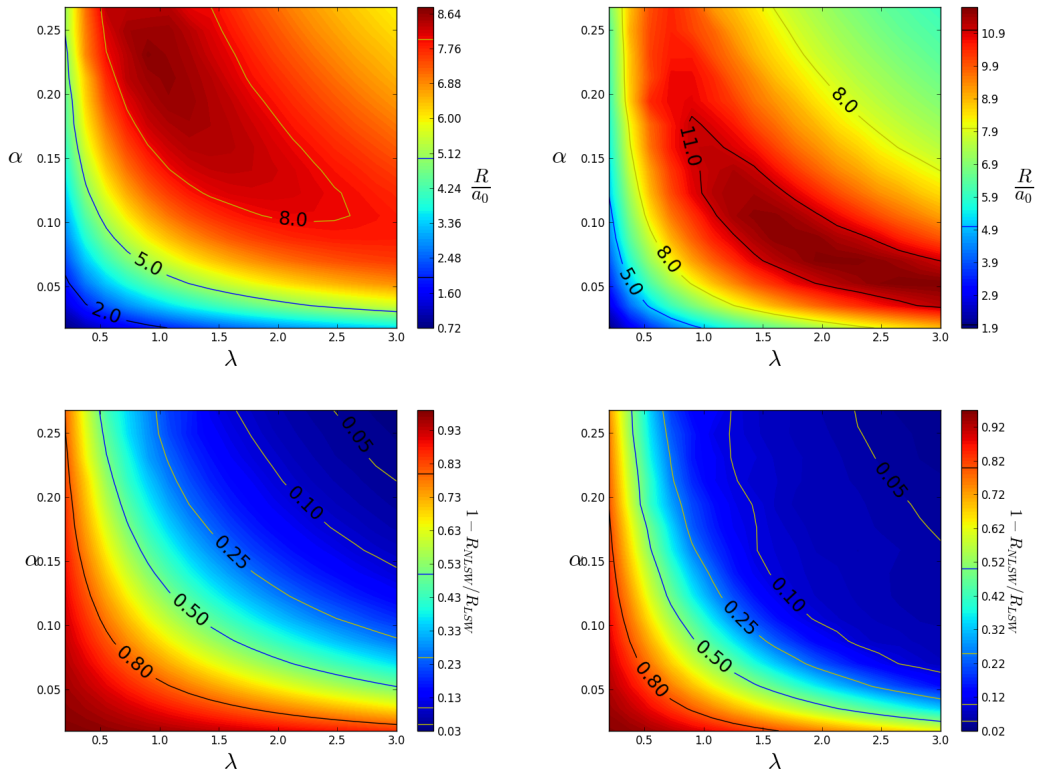

Figure 7.6: Top row: Relative run-up heights for NLSW using geoCLAW for $h_1 = 0.9$. Bottom row: Relative difference between LSW and NLSW. In the left column the friction coefficient $\gamma = 0.025$ and in the right column $\gamma = 0$.

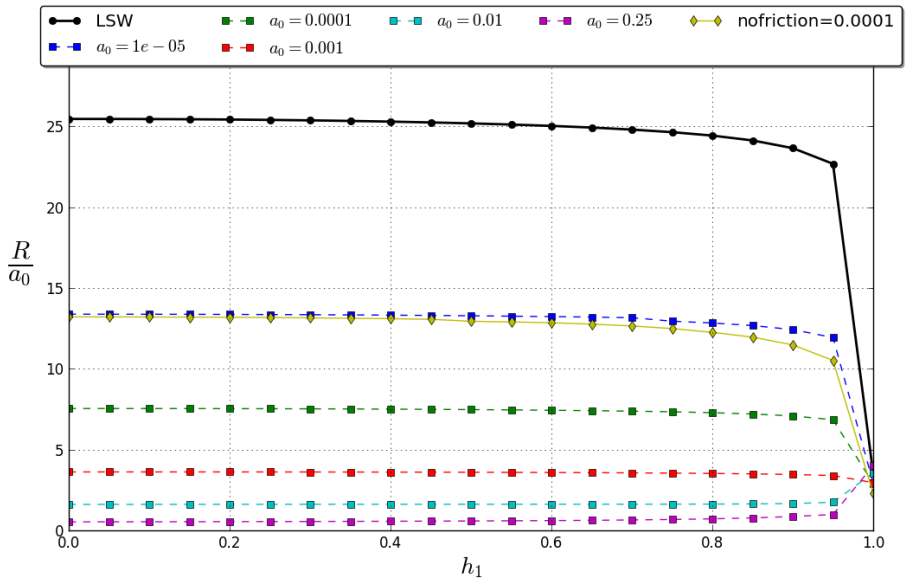

Figure 7.7: Relative run-up height for wave with $\lambda = 3$ as a function of h_1 with $\alpha = 1°$.

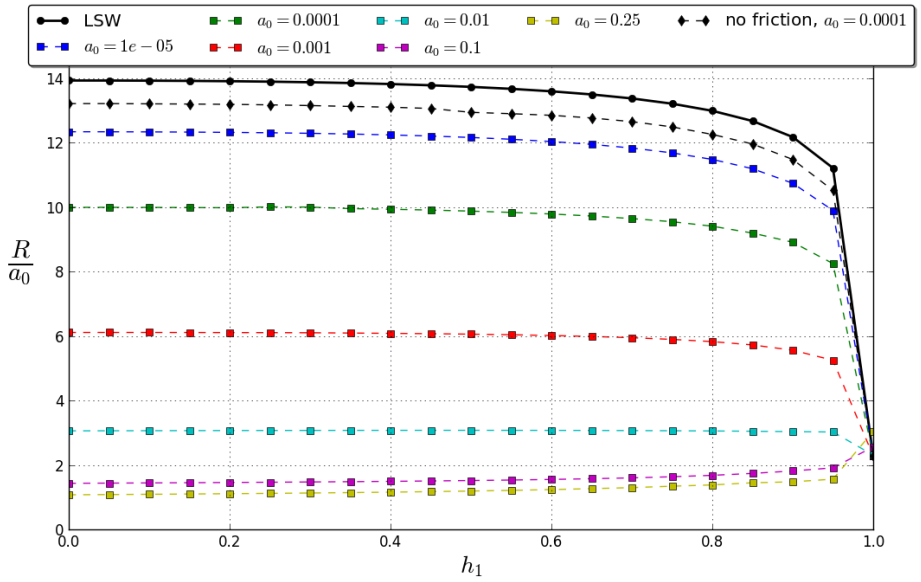

Figure 7.8: Relative run-up height for wave with $\lambda = 10$ as a function of h_1 with $\alpha = 1°$.

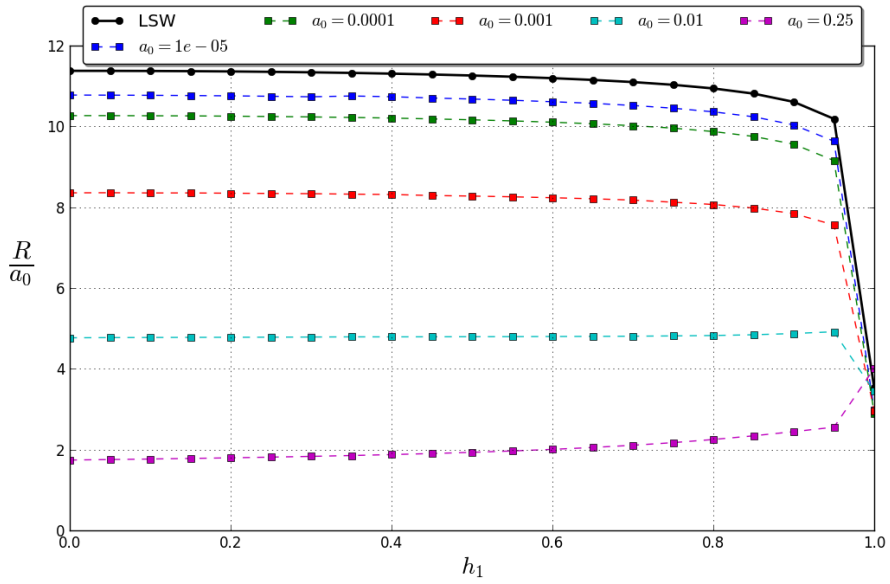

Figure 7.9: Relative run-up height for wave with $\lambda = 3$ as a function of h_1 with $\alpha = 5°$.

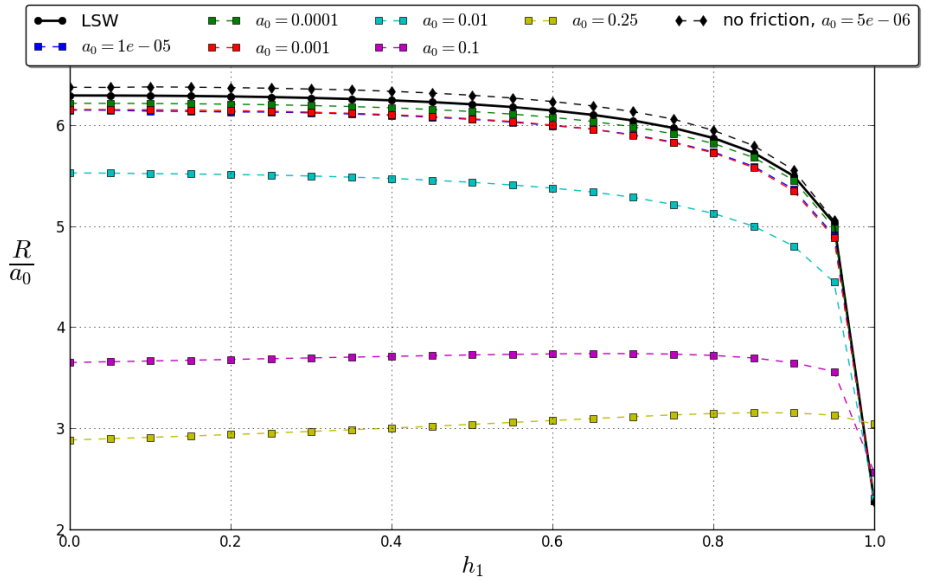

Figure 7.10: Relative run-up height for wave with $\lambda = 10$ as a function of h_1 with $\alpha = 5°$.

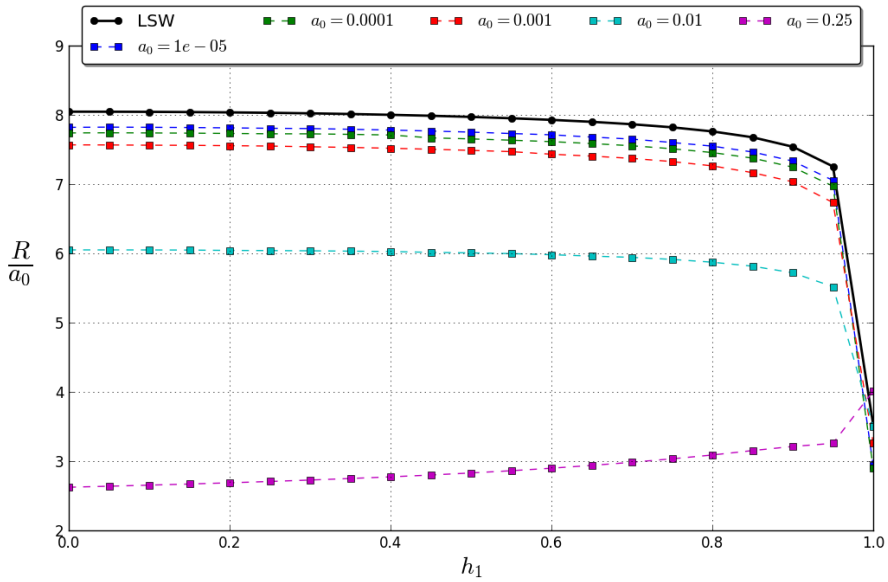

Figure 7.11: Relative run-up height for wave with $\lambda = 3$ as a function of h_1 with $\alpha = 10°$.

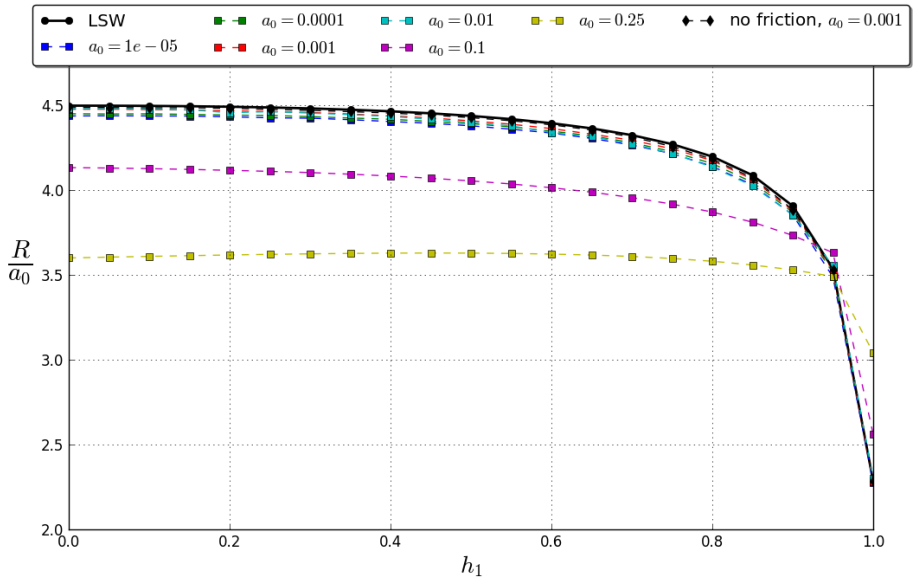

Figure 7.12: Relative run-up height for wave with $\lambda = 10$ as a function of h_1 with $\alpha = 10°$.

Chapter 8

Summary and Conclusion

In this thesis, run-up of periodic and single waves have been investigated. The main focus have been to determine which part of a composite slope is crucial for the run-up height of an incident wave. The results have been obtained by numerical simulations for a vast amount of parameter combinations and different solvers have been used the various problems. Two linear solvers have been implemented by the author and an open source NLSW solver including terms for the bottom friction have also been used. Findings related to the run-up process such as wave reflection due to the slope and the effects of an offshore area much longer than the incident waves wavelength have also been reported.

The main findings can be summarized as

- The run-up height for breaking waves seems to be determined by the slope parameters in the region where the depth approaches zero.
- Increased steepness of a non-breaking nonlinear wave increases the run-up height.
- The run-up height for linear single waves show only minor differences ($\sim$ 1%) if the sharp vertex connecting the constant depth region to the slope are replaced by a smooth transition. However, the shape and amplitude of the reflected wave are significantly more affected and may result in earlier

breaking for non-linear waves.

- The optic approximation is a good approximation very close to the shoreline for a single plane geometry
- The run-up height of linear periodic waves on a composite slope is only affected by the slope segment closest to the shoreline for values of $h_1/h_0 \approx 0.5$. For the shorter wavelengths the run-up height appears little affected by the first slope segment even for values of $h_1/h_0 = 0.9$. However, the occurrence of extrema in the run-up function makes the estimate less accurate for specific wavelengths as h_1/h_0 increases. We do note that the mean value of the extrema yields results with little error.
- The run-up height for linear single waves also seems little affected by the first slope segment for values of $h_1/h_0 \sim 0.5$. The estimate is better for shorter wavelengths. The same applies for strictly non-breaking nonlinear waves with and without bottom friction included.

8.1 Future Work

A natural next step is to expand the calculations to include 2 horizontal dimensions. An investigation should be made into the similarity of the occurrence of extrema for waves on a composite slope and waves with an oblique angle of incidence on a straight beach. Refraction of single waves due to the slope and it's effects on the run-up height are also of interest. Including of the dispersive terms should also be investigated.

Appendices

Appendix A

Convergence and stability

A.1 LSW - time plane

It can be shown that the discrete LSW equations is of second order by a simple Taylor expansion around the point where we want to perform the differentiation. First we Taylor expand from $(i + \frac{1}{2})\Delta x$ around $i\Delta x$

$$f\left(\left(i+\frac{1}{2}\right)\Delta x\right) \approx f(i\Delta x)+\frac{\Delta x}{2}f'(i\Delta x)+\left(\frac{\Delta x}{2}\right)^2 f''(i\Delta x)+\mathcal{O}\left(\left(\frac{\Delta x}{2}\right)^3\right) \quad \text{(A.1)}$$

The we Taylor expand from $(i - \frac{1}{2})\Delta x$ around $i\Delta x$

$$f\left(\left(i-\frac{1}{2}\right)\Delta x\right) \approx f(i\Delta x)-\frac{\Delta x}{2}f'(i\Delta x)+\left(\frac{\Delta x}{2}\right)^2 f''(i\Delta x)-\mathcal{O}\left(\left(\frac{\Delta x}{2}\right)^3\right) \quad \text{(A.2)}$$

Subtracting these series from one another yields

$$f\left(\left(i+\frac{1}{2}\right)\Delta x\right)-f\left(\left(i-\frac{1}{2}\right)\Delta x\right)=\Delta x f'(i\Delta x)+\frac{1}{4}\mathcal{O}\left((\Delta x)^3\right) \tag{A.3}$$

As $\Delta x \to 0$ the constant infront of the truncation error $\mathcal{O}$ becomes redundant. Dividing both sides with Δx yields

$$f'(i\Delta x)=\frac{f\left(\left(i+\frac{1}{2}\right)\Delta x\right)-f\left(\left(i-\frac{1}{2}\right)\Delta x\right)}{\Delta x}+\mathcal{O}\left((\Delta x)^2\right) \tag{A.4}$$

Inserting the exact solutions from Pedersen [16]

$$\eta=\hat{\eta}e^{i(kx-\omega t)} \qquad u=\hat{u}e^{i(kx-\omega t)} \tag{A.5}$$

into the LSW we obtain the relations

$$\begin{aligned}\omega&=\sqrt{h_0}k\\ \hat{\eta}&=\sqrt{h_0}\hat{u}\end{aligned} \tag{A.6}$$

Utilizing these relations combined with the discrete exact solutions in the discrete LSW we obtain the numerical dispersion relation

$$\sin\left(\frac{\omega\Delta t}{2}\right)=C_0\sin\left(\frac{k\Delta x}{2}\right) \tag{A.7}$$

where $C_0=\sqrt{h_0}\frac{\Delta t}{\Delta x}$. This must be valid for any k. By choosing $k=\frac{\pi}{\Delta x}$ we obtain

$$\left|\sin\left(\frac{\omega\Delta t}{2}\right)\right|=C_0\leq 1 \tag{A.8}$$

and thus, for problems related to this thesis where $h_0=1$, the stability conditions reads

$$\Delta t\leq\Delta x \tag{A.9}$$

By utilizing (A.6) in Eq.(A.7) it shows that the dispersion relation is exact for $\Delta x=\Delta t$

$$\sin\left(\frac{k\Delta t}{2}\right)=\sin\left(\frac{k\Delta x}{2}\right) \tag{A.10}$$

Appendix B

Tables and Figures

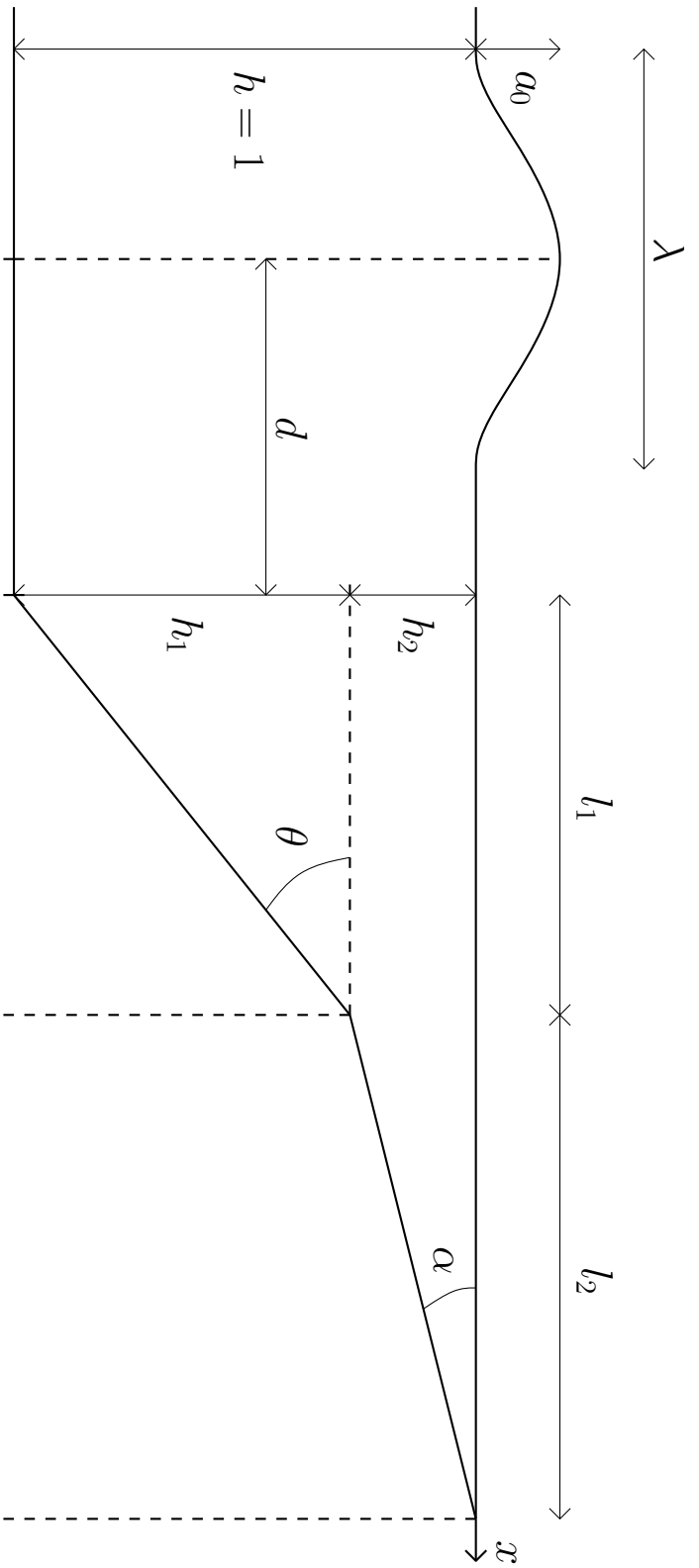

Figure B.1: Composite slope bathymetry. All parameters are non-dimensional. Offshore region defined as $x_0 \leq x < x_k$. Nearshore region defined as $x_k \leq x \leq x_S$.

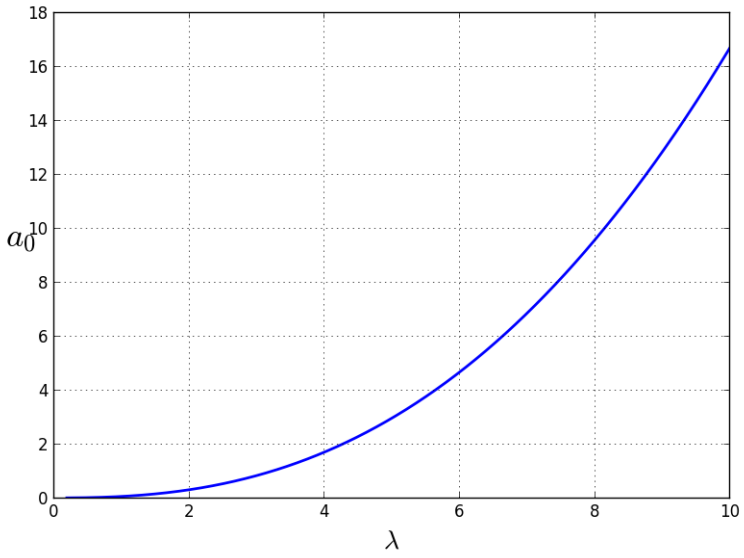

Figure B.2: Breaking parameter for $\tan(\theta) = 1$

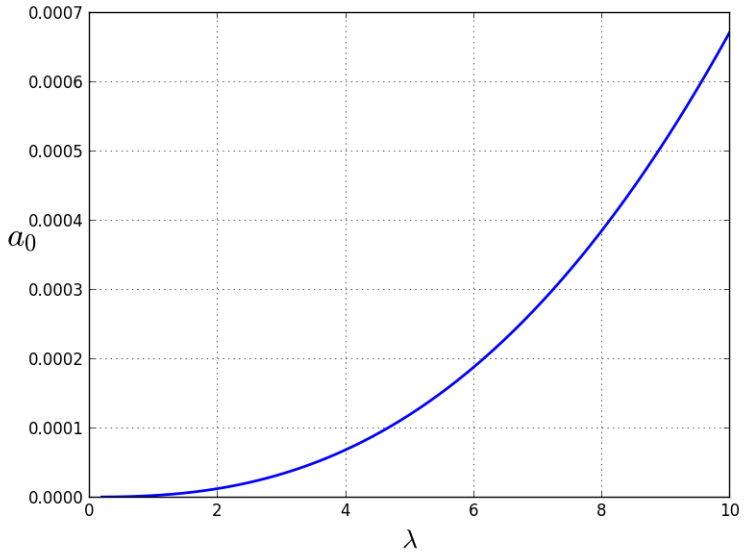

Figure B.3: Breaking parameter for $\tan(\theta) = 0.017$

Bibliography

[1] M. J. Berger, D. L. George, R. J. LeVeque, and K. T. Mandli. "The GeoClaw software for depth-averaged flows with adaptive refinement". In: *Adv. Water Res.* 34 (2011), pp. 1195–1206. URL: %5Curl%7Bwww.clawpack.org/links/papers/awr11%7D.

[2] GF Carrier and HP Greenspan. "Water waves of finite amplitude on a sloping beach". In: *Journal of Fluid Mechanics* 4.01 (1958), pp. 97–109.

[3] Ira Didenkulova. "New trends in the analytical theory of long sea wave runup". In: *Applied Wave Mathematics*. Springer, 2009, pp. 265–296.

[4] B. Gjevik, G. K. Pedersen, and K. Trulsen. *Forelesninger i bølgeteori*. Matematisk Institutt, Universitetet i Oslo, (2015).

[5] Bjørn Gjevik and Geir Pedersen. "Run-up of long waves on an inclined plane". In: *Preprint series. Mechanics and Applied Mathematics http://urn.nb. no/URN: NBN: no-23418* (1981).

[6] Google Earth Engine Team. *Google Earth Engine: A planetary-scale geospatial analysis platform*. https://earthengine.google.com. Dec. 2015.

[7] U. Kânoğlu and C. E. Synolakis. "Long wave runup on piecewise linear topographies". In: *J. Fluid Mech* 374 (1998), pp. 1–28.

[8] R. J. LeVeque. *Finite Volume Methods for Hyperbolic Problems*. Cambridge University Press, 2002. URL: http://www.clawpack.org/book.html.

[9] R.J. LeVeque, D. L. George, and M. J. Berger. "Adaptive Mesh Refinement Techniques for Tsunamis and Other Geophysical Flows Over Topography". In: *Acta Numerica* (2011), pp. 211–289.

[10] Jibin Li and Zhengrong Liu. "Smooth and non-smooth traveling waves in a nonlinearly dispersive equation". In: *Applied Mathematical Modelling* 25.1 (2000), pp. 41–56.

[11] Per A Madsen, David R Fuhrman, and Hemming A Schäffer. "On the solitary wave paradigm for tsunamis". In: *Journal of Geophysical Research: Oceans* 113.C12 (2008).

[12] Yoshinobu Ogawa and Nobuo Shuto. "Run-up of periodic waves on beaches of non-uniform slope". In: *Coastal Engineering 1984*. 1985, pp. 328–344.

[13] G Pedersen. "Fully nonlinear Boussinesq equations for long wave propagation and run-up in sloping channels with parabolic cross sections". In: *Natural Hazards* 84.2 (2016), pp. 599–619.

[14] G Pedersen. "Modeling runup with depth integrated equation models". In: *Advanced numerical models for simulating tsunami waves and runup* 10 (2008), pp. 3–42.

[15] G. K. Pedersen. *A program for the standard Boussinesq equation*. `http://folk.uio.no/geirkp/bouss/index.html`. Accessed: 2016-11-01.

[16] G. K. Pedersen. *Numerical investigations on nonlinear and dispersive wave propagation*. `http://folk.uio.no/geirkp/bouss/exercises.pdf`. Accessed: 2016-2-15.

[17] G Pedersen and B Gjevik. "Run-up of solitary waves". In: *Journal of fluid mechanics* 135 (1983), pp. 283–299.

[18] Geir Pedersen. "Run-up of periodic waves on a straight beach". In: *Preprint series. Mechanics and Applied Mathematics http://urn. nb. no/URN: NBN: no-23418* (1985).

[19] EN Pelinovsky and R Kh Mazova. "Exact analytical solutions of nonlinear problems of tsunami wave run-up on slopes with different profiles". In: *Natural Hazards* 6.3 (1992), pp. 227–249.

[20] K. Rottmann. *Matematisk formelsamling*. Spektrum forlag, (2013). ISBN: 978-1-118-47580-5.

[21] Costas Emmanuel Synolakis. "Green's law and the evolution of solitary waves". In: *Physics of Fluids A: Fluid Dynamics* 3.3 (1991), pp. 490–491.

[22] Costas Emmanuel Synolakis. "The runup of solitary waves". In: *Journal of Fluid Mechanics* 185 (1987), pp. 523–545.

[23] Clawpack Development Team. *Clawpack software*. Version 5.4.0. 2017. URL: `http://www.clawpack.org`.

[24] Aslak Tveito, Hans Petter Langtangen, Bjørn Frederik Nielsen, and Xing Cai. *Elements of scientific computing*. Vol. 7. Springer Science & Business Media, 2010.

[25] Aslak Tveito and Ragnar Winther. *Introduction to partial differential equations: a computational approach*. Vol. 29. Springer Science & Business Media, 2004.